DUKE UNIVERSITY

Department of Electrical Engineering
School of Engineering

Final Report
October 1, 1989 - February 14, 1991
Grant No. N00014-90-J-1018

ADAPTIVE ACOUSTIC SIGNAL DETECTION

DUKE UNIVERSITY

Department of Electrical Engineering
School of Engineering

Final Report
October 1, 1989 - February 14, 1991
Grant No. N00014-90-J-1018

ADAPTIVE ACOUSTIC SIGNAL DETECTION

Approved: L. W. Nolte

L. W. Nolte, Principal Investigator

Prepared under: Office of Naval Research (Code 1125OA)
Grant No. N00014-90-J-1018

Contents

List of Figures

1 Introduction

The focus of this research is to determine the impact of our knowledge of ocean variability, as characterized by the sound speed profile, on ocean surveillance detection performance for situations of interest to the U. S. Navy. Signal detection theory provides a framework for determining optimal phase coherent detection and source localization algorithms and determining their performance. This framework allows us to incorporate directly the physics of acoustic propagation through a space-time variable medium into the structure of optimal algorithms. Thus the signal processing algorithms designed from this viewpoint have a built-in robustness to the environmental variability. Using these optimal algorithms we can determine the maximum attainable detection performance.

2 Approach

Our approach is a combination of theory, some very computationally intensive numerical work, and the use of real sound speed profiles, where appropriate, obtained from the ocean acoustics community. The approach is to use the framework of signal detection theory to obtain optimal algorithms for inhomogeneous and stochastic ocean models characterized by an ensemble of sound speed profiles. Ideally, we would like to compute the detection and localization performance for a volume of received points as a function of a large volume of possible source locations, for varying degrees of knowledge of an uncertain, inhomogeneous and stochastic ocean medium. Available software codes and computational speeds limit the complexity of situations that can be considered. The approach requires: (a) setting up a meaningful sound speed profile description of the ocean; (b) incorporating the variabilities and stochastic nature of the ocean in the description of the ensemble of sound speed profiles, as well as uncertainties of source signal characteristics, source position, and noise; (c) solving for the received fields as a function of all possible source locations; (d) using the received fields to generate the optimal detection and localization algorithms for a given ocean acoustic scenario (i.e. the likelihood ratio for the detection problem and the a posteriori probability for the source localization and the tomography problem); and (e) obtaining the detection and localization performance of these optimal algorithms to get

the maximum obtainable performance.

Our approach has been to exploit the ability to remotely sense the sound velocity profile of the ocean, as demonstrated by the ocean acoustic tomography group of Scripps/Woods Hole/Univ. of Michigan/APL. A very important issue is to determine what the attainable surveillance detection performance is given that one has a more detailed description of how sound is propagated in an inhomogeneous ocean environment, in the deep ocean, at long ranges. Signal detection theory provides a framework for determining optimal detection algorithms and their performance. In other words, we are able to utilize the knowledge that the ocean tomography group is able to obtain in regard to the sound speed profile and use that physics to determine the changing wavefront of the propagating signal in an inhomogeneous ocean environment. This information is used to drive the structure of optimal algorithms from which we can obtain the maximum attainable detection performance.

3 Summary of Research Accomplished

Results have been obtained in:

- Development of new a posteriori probability source localization algorithms by Richardson and Nolte [10, 11]. These algorithms, unlike matched field processing algorithms, do not require complete knowledge of the acoustic environment, but can determine source position even with uncertain or imprecise information about the environment. This algorithm is termed the optimum uncertain field processing (OUFP) algorithm.

  Paramer estimation theory is utilized to derive the new algorithm. THis provides a systematic, optimal approach to the problem, and allows environmental uncertainty to be easilyincorporated into the algorithm. In addition to estimating source position, estimates of parameters of the acoustic environment can also be calculated. This makes simultaneous source localization and acoustic tomographic estimation of ocean parameters possible.

  A series of results, some of which are presented here, illustrate the robust performance of the uncerain field processor, relative to the per-

formance of matched field processing methods. Estimation of ocean acoustic parameters is also illustrated.

- Development of optimum ocean-model-based detection algorithms by Lazoff [8]. Effects of signal bandwidth on detection performance of optimal ocean-model-based algorithms, for signals received through an inhomogeneous acoustic ocean medium.

- Sensitivity of wide band matched-field localization to the sound speed profile information by Clarke and Rausch [2, 12].

4 Results-Optimal Acoustic Source Localization Algorithm

The problem of localization in cases in which there is uncertainty about the parameters describing the acoustic environment is considered by Richardson [10, 11]. This is a generalization of the problem in which it is desired to locate a source in a known or certain environment (the matched field problem), which has received considerable attention in the literature since Bucker's 1976 paper [1].

The sensitivity of matched field algorithms to environmental uncertainty has been illustrated in various studies [1, 9, 3, 13, 10]. These studies indicate that matched field localization algorithms can be quite sensitive to mismatch between the actual environment and that for which the algorithms are designed.

By considering the more general problem, we can design new algorithms which we hope are less sensitive to mismatch. Since the known environment is a limiting case of the uncertain environment, valuable insight is gained into the matched field problem.

The source localization problem is regarded as a problem in parameter estimation theory. The source position coordinates (range, depth and bearing) are treated as unknown parameters of the observed acoustic field. Parameter estimation theory provides the necessary framework for the design of an optimum algorithm for estimating source position. This algorithm is termed the optimum uncertain field processor (OUFP). The main advantages of this approach are: (1) it provides a framework for the development of optimum localization algorithms, (2) it introduces well understood performance measures for comparison of different algorithms, and (3) it allows probabilistic descriptions of environmental uncertainty to be easily incorporated into the problem.

4.1 Notation

The observation (or measurement) consists of K time samples from each of N elements of a receive array. The vector $\mathbf{r}_k$ represents a snapshot of the element outputs at time sample k. The complete observation is arranged as

an $NK \times 1$ matrix (column vector),

$$\mathbf{r} = [\mathbf{r}_1^T : \mathbf{r}_2^T : \cdots : \mathbf{r}_K^T]^T. \tag{1}$$

The observation consists of signal and additive noise components,

$$\mathbf{r} = \mathbf{s}(\mathbf{S}, \mathbf{\Phi}, \mathbf{\Psi}) + \mathbf{w}. \tag{2}$$

We assume that the signal component depends upon several parameters, some of which are unknown. The set of source position parameters (e.g., range, depth, and bearing) is denoted $\mathbf{S}$. Any parameters describing the transmitted pressure waveform (e.g., amplitude, phase, center frequency, etc.) are denoted $\mathbf{\Phi}$. Parameters which are required to describe the acoustic medium (e.g., any sound velocity profile parameters, descriptions of the boundary conditions, etc.) are collectively denoted $\mathbf{\Psi}$.

4.2 The General OUFP Equation

The range, depth and bearing of the source are treated as random variables. The optimum uncertain field processor is defined as the implementation of the source position a posteriori probability density function. Source and environment uncertainty, as expressed by probability density functions, can easily be included into the problem. This definition is intuitively meaningful and allows many of the classical estimators (for example, minimum mean-square error, maximum a posteriori, maximum likelihood, etc.) to be calculated.

The source position a posteriori probability density function (pdf), $p_{\mathbf{S}|\mathbf{r}}(\mathbf{S}|\mathbf{r})$, is related to the conditional observation pdf, $p_{\mathbf{r}|\mathbf{S}}(\mathbf{r}|\mathbf{S})$ by

$$p_{\mathbf{S}|\mathbf{r}}(\mathbf{S}|\mathbf{r}) = \frac{p_{\mathbf{S}}(\mathbf{S})}{p_{\mathbf{r}}(\mathbf{r})} p_{\mathbf{r}|\mathbf{S}}(\mathbf{r}|\mathbf{S}). \tag{3}$$

Only the case in which the observation is a deterministic function of the transmitted waveform and $\mathbf{S}$ and $\mathbf{\Psi}$ is considered here (the deterministic ocean model). The transmitted signal is assumed to be completely determined if $\mathbf{\Phi}$ is known (the deterministic signal case). The pdf describing the observation is then related to the noise pdf by

$$p_{\mathbf{r}|\mathbf{S},\mathbf{\Phi},\mathbf{\Psi}}(\mathbf{r}|\mathbf{S}, \mathbf{\Phi}, \mathbf{\Psi}) = p_{\mathbf{w}}(\mathbf{r} - \mathbf{s}(\mathbf{S}, \mathbf{\Phi}, \mathbf{\Psi})). \tag{4}$$

(This equation is not applicable if either the transmitted signal or the acoustic transfer function are random).

From the definition of conditional probability density functions we can write

$$p_{\mathbf{r},\mathbf{\Phi},\mathbf{\Psi}|\mathbf{S}}(\mathbf{r},\mathbf{\Phi},\mathbf{\Psi}|\mathbf{S}) = p_{\mathbf{r}|\mathbf{S},\mathbf{\Phi},\mathbf{\Psi}}(\mathbf{r}|\mathbf{S},\mathbf{\Phi},\mathbf{\Psi})p_{\mathbf{\Phi},\mathbf{\Psi}|\mathbf{S}}(\mathbf{\Phi},\mathbf{\Psi}|\mathbf{S}), \tag{5}$$

or

$$p_{\mathbf{r},\mathbf{\Phi},\mathbf{\Psi}|\mathbf{S}}(\mathbf{r},\mathbf{\Phi},\mathbf{\Psi}|\mathbf{S}) = p_{\mathbf{w}}(\mathbf{r}-\mathbf{s}(\mathbf{S},\mathbf{\Phi},\mathbf{\Psi}))p_{\mathbf{\Phi},\mathbf{\Psi}|\mathbf{S}}(\mathbf{\Phi},\mathbf{\Psi}|\mathbf{S}). \tag{6}$$

We can obtain $p_{\mathbf{r}|\mathbf{S}}(\mathbf{r}|\mathbf{S})$ by integrating this density function over $\mathbf{\Phi}$ and $\mathbf{\Psi}$,

$$p_{\mathbf{r}|\mathbf{S}}(\mathbf{r}|\mathbf{S}) = \int_{\mathbf{\Psi}}\int_{\mathbf{\Phi}} p_{\mathbf{w}}(\mathbf{r}-\mathbf{s}(\mathbf{S},\mathbf{\Phi},\mathbf{\Psi}))p_{\mathbf{\Phi},\mathbf{\Psi}|\mathbf{S}}(\mathbf{\Phi},\mathbf{\Psi}|\mathbf{S})\,d\mathbf{\Phi}\,d\mathbf{\Psi}. \tag{7}$$

Finally, the desired a posteriori source position pdf can be obtained by substitution of this expression into Eq. 3,

$$p_{\mathbf{S}|\mathbf{r}}(\mathbf{S}|\mathbf{r}) = \frac{p_{\mathbf{S}}(\mathbf{S})}{p_{\mathbf{r}}(\mathbf{r})}\int_{\mathbf{\Psi}}\int_{\mathbf{\Phi}} p_{\mathbf{w}}(\mathbf{r}-\mathbf{s}(\mathbf{S},\mathbf{\Phi},\mathbf{\Psi}))p_{\mathbf{\Phi},\mathbf{\Psi}|\mathbf{S}}(\mathbf{\Phi},\mathbf{\Psi}|\mathbf{S})\,d\mathbf{\Phi}\,d\mathbf{\Psi}. \tag{8}$$

This is the defining equation of the optimum uncertain field processor. It can be simplified in many applications of interest, as shown in the next subsection.

4.3 The Narrowband Signal in Gaussian Noise Problem

Matched field processing methods have concentrated on localizing a narrowband source in the presence of a Gaussian noise background. It is this problem to which we now turn our attention.

If the elements of the noise component of the observation are Gaussian distributed and jointly stationary, the noise probability density function is given by

$$p_{\mathbf{w}}(\mathbf{w}) = \frac{1}{(2\pi)^{NK/2}|\mathbf{\Omega}|^{1/2}}\exp\left(-\frac{1}{2}\mathbf{w}^T\mathbf{\Omega}^{-1}\mathbf{w}\right). \tag{9}$$

$\mathbf{\Omega}$ is the space-time noise covariance matrix and $|\mathbf{\Omega}|$ is its determinant. The conditional pdf of the observation can therefore be written as

$$p_{\mathbf{r}|\mathbf{S},\mathbf{\Phi},\mathbf{\Psi}}(\mathbf{r}|\mathbf{S},\mathbf{\Phi},\mathbf{\Psi}) = \frac{\exp\left(-\frac{1}{2}\mathbf{r}^T\mathbf{\Omega}^{-1}\mathbf{r}\right)}{(2\pi)^{NK/2}|\mathbf{\Omega}|^{1/2}}\exp\left(\Lambda(\mathbf{S},\mathbf{\Phi},\mathbf{\Psi},\mathbf{r})\right), \tag{10}$$

where

$$\Lambda(\mathbf{S}, \mathbf{\Phi}, \mathbf{\Psi}, \mathbf{r}) = \mathbf{r}^T \mathbf{\Omega}^{-1} \mathbf{s} - \frac{1}{2} \mathbf{s}^T \mathbf{\Omega}^{-1} \mathbf{s}. \tag{11}$$

(For convenience, the explicit notational dependence of $\mathbf{s}$ upon $\mathbf{S}$, $\mathbf{\Phi}$, and $\mathbf{\Psi}$ has been dropped.)

The source position a posteriori pdf is equal to

$$p_{\mathbf{S}|\mathbf{r}}(\mathbf{S}|\mathbf{r}) = C(\mathbf{r}) p_{\mathbf{S}}(\mathbf{S}) \int_{\mathbf{\Psi}} \int_{\mathbf{\Phi}} \exp\left(\Lambda(\mathbf{S}, \mathbf{\Phi}, \mathbf{\Psi}, \mathbf{r})\right) p_{\mathbf{\Phi},\mathbf{\Psi}|\mathbf{S}}(\mathbf{\Phi}, \mathbf{\Psi}|\mathbf{S}) \, d\mathbf{\Phi} \, d\mathbf{\Psi}, \tag{12}$$

where $C(\mathbf{r})$ is some function of $\mathbf{r}$ (the functional relationship is of no significance) that reduces to a normalization constant for any particular observation.

The problem is simplified if the noise samples are uncorrelated in time. The matrix $\mathbf{\Omega}$ can then be written as the Kronecker product of the spatial covariance matrix, $\mathbf{Q}$, and a $K \times K$ identity matrix, $\mathbf{I}_{KK}$, that is,

$$\mathbf{\Omega} = \mathbf{Q} \otimes \mathbf{I}_{KK}. \tag{13}$$

(The Kronecker product is the $NO \times MP$ matrix which results from the element by element multiplication of an $N \times M$ by an $O \times P$ matrix.) The following set of equations are easily derived from the properties the Kronecker product,

$$\mathbf{\Omega}^{-1} = \mathbf{Q}^{-1} \otimes \mathbf{I}_{KK} \tag{14}$$

$$\mathbf{r}^T \mathbf{\Omega}^{-1} \mathbf{s} = \sum_{k=1}^{K} \mathbf{r}_k^T \mathbf{Q}^{-1} \mathbf{s}_k \tag{15}$$

$$\mathbf{s}^T \mathbf{\Omega}^{-1} \mathbf{s} = \sum_{k=1}^{K} \mathbf{s}_k^T \mathbf{Q}^{-1} \mathbf{s}_k. \tag{16}$$

Eq. 11 can then be written as

$$\Lambda(\mathbf{S}, \mathbf{\Phi}, \mathbf{\Psi}, \mathbf{r}) = \sum_{k=1}^{K} \left[\mathbf{r}_k^T \mathbf{Q}^{-1} \mathbf{s}_k - \frac{1}{2} \mathbf{s}_k^T \mathbf{Q}^{-1} \mathbf{s}_k \right] \tag{17}$$

An eigenvector decomposition of the spatial covariance matrix can be represented by

$$\mathbf{Q} = \sum_{n=1}^{N} \lambda_n \mathbf{q}_n \mathbf{q}_n^T, \tag{18}$$

where the $\mathbf{q}_n$ are the eigenvectors of $\mathbf{Q}$ and the λ_n are the corresponding eigenvalues. This can be used to rewrite Eq. 17 as

$$\Lambda(\mathbf{S}, \mathbf{\Phi}, \mathbf{\Psi}, \mathbf{r}) = \sum_{n=1}^{N} \lambda_n^{-1} \mathbf{q}_n^T \left[\sum_{k=1}^{K} \left(\mathbf{s}_k \mathbf{r}_k^T - \frac{1}{2} \mathbf{s}_k \mathbf{s}_k^T \right) \right] \mathbf{q}_n. \tag{19}$$

A transmitted narrowband pressure waveform has the form

$$x(t) = A \cos(\omega_0 t + \theta). \tag{20}$$

The transmitted amplitude and phase are assumed to be unknown parameters of the transmitted waveform; i.e., they are members of the set $\mathbf{\Phi}$.

The acoustic transfer function between the source and array element n can be written as

$$H_n(\mathbf{S}, \mathbf{\Psi}) = a_n(\mathbf{S}, \mathbf{\Psi}) e^{i\theta_n(\mathbf{S}, \mathbf{\Psi})}. \tag{21}$$

The transfer function depends only upon the source position and the parameters of the environment.

The signal component of the observation is therefore equal to

$$s_{nk} = A a_n \cos(\omega_0 t_k + \theta_n + \theta). \tag{22}$$

The outer product terms in Eq. 19 can now be evaluated. The element of the matrix $\sum_{k=1}^{K} \mathbf{s}_k \mathbf{s}_k^T$ in row n and column n' is equal to

$$\left[\sum_{k=1}^{K} \mathbf{s}_k \mathbf{s}_k^T \right]_{nn'} = A^2 a_n a_{n'} \sum_{k=1}^{K} \cos(\omega_0 t_k + \theta_n + \theta) \cos(\omega_0 t_k + \theta_{n'} + \theta). \tag{23}$$

If the sampling interval is much less than the signal period, the summation may be approximated as an integral. This results in

$$\left[\sum_{k=1}^{K} \mathbf{s}_k \mathbf{s}_k^T \right]_{nn'} = \frac{A^2 K a_n a_{n'}}{T} \int_0^T \cos(\omega_0 t + \theta_n + \theta) \cos(\omega_0 t + \theta_{n'} + \theta)\, dt, \tag{24}$$

where T is the observation time. A trigonometric identity reduces this to

$$\left[\sum_{k=1}^{K} \mathbf{s}_k \mathbf{s}_k^T \right]_{nn'} = \frac{A^2 K a_n a_{n'}}{2T} \times \int_0^T \cos(\theta_n - \theta_{n'}) + \cos(2\omega_0 t + 2\theta + \theta_n + \theta_{n'})\, dt. \tag{25}$$

Assuming that the observation time is over several periods of the observation, the integral over the second term is negligible when compared to the first and we have

$$\left[\sum_{k=1}^{K} \mathbf{s}_k \mathbf{s}_k^T\right]_{nn'} = \frac{A^2 K}{2} a_n a_{n'} \cos(\theta_n - \theta_{n'}). \tag{26}$$

Rewriting this in terms of the acoustic transfer function yields

$$\left[\sum_{k=1}^{K} \mathbf{s}_k \mathbf{s}_k^T\right]_{nn'} = \frac{A^2 K}{2} \Re\left\{H_n H_n^*\right\}. \tag{27}$$

The entire matrix can therefore be written as

$$\sum_{k=1}^{K} \mathbf{s}_k \mathbf{s}_k^T = \frac{A^2 K}{2} \Re\left\{\mathbf{H}\mathbf{H}^*\right\}, \tag{28}$$

where $\mathbf{H}$ is an N element column vector whose elements are given by Eq. 21.

Turning to the other outer product term, an element of the matrix, $\sum_{k=1}^{K} \mathbf{s}_k \mathbf{r}_k^T$, is equal to

$$\left[\sum_{k=1}^{K} \mathbf{s}_k \mathbf{r}_k^T\right]_{nn'} = A \sum_{k=1}^{K} r_{n'}(t_k) a_n \cos(\omega_0 t_k + \theta_n + \theta). \tag{29}$$

Again approximating the summation by an integral results in

$$\left[\sum_{k=1}^{K} \mathbf{s}_k \mathbf{r}_k^T\right]_{nn'} = \frac{AK}{T} \int_0^T r_{n'}(t) a_n \cos(\omega_0 t + \theta_n + \theta)\, dt, \tag{30}$$

which can be written in complex notation as

$$\left[\sum_{k=1}^{K} \mathbf{s}_k \mathbf{r}_k^T\right]_{nn'} = \frac{AK}{\sqrt{2}} \Re\left\{e^{i\theta} a_n e^{i\theta_n} \frac{\sqrt{2}}{T} \int_0^T r_{n'}(t) e^{i\omega_0 t}\, dt\right\}. \tag{31}$$

The notation can be simplified by rewriting this as

$$\left[\sum_{k=1}^{K} \mathbf{s}_k \mathbf{r}_k^T\right]_{nn'} = \frac{A\sigma_A K}{\sqrt{2}} \Re\left\{e^{i\theta} H_n P_{n'}^*\right\}, \tag{32}$$

where $P_{n'}$ is defined as

$$P_{n'} = \frac{\sqrt{2}}{\sigma_A T} \int_0^T r_{n'}(t) e^{-i\omega_0 t}\, dt, \tag{33}$$

and σ_A is a normalization factor that will be defined shortly. The complete matrix is therefore equal to

$$\sum_{k=1}^{K} \mathbf{s}_k \mathbf{r}_k^T = \frac{A\sigma_A K}{\sqrt{2}} \Re\left\{ e^{i\theta} \mathbf{H}\mathbf{P}^* \right\}. \tag{34}$$

The vector $\mathbf{P}$ is an N element column vector whose elements are defined in Eq. 33.

Substituting Eqs. 28 and 34 into Eq. 19 and recalling Eq. 18 results in

$$\Lambda(\mathbf{S}, \mathbf{\Phi}, \mathbf{\Psi}, \mathbf{r}) = -\frac{A^2}{2\sigma_A^2} E + \frac{\sqrt{2}A}{\sigma_A} \Re\left\{ R e^{i\theta} \right\}, \tag{35}$$

where

$$E = \frac{\sigma_A^2 K}{2} \mathbf{H}^* \mathbf{Q}^{-1} \mathbf{H} \tag{36}$$

$$R = \frac{\sigma_A^2 K}{2} \mathbf{H}^* \mathbf{Q}^{-1} \mathbf{P}. \tag{37}$$

R indicates to what degree the measured field, $\mathbf{P}$, is similar to the matching field, $\mathbf{H}$. E is a normalization term which is proportional to the self-energy in the matching field. Both R and E are functions of $\mathbf{S}$, $\mathbf{\Phi}$ and $\mathbf{\Psi}$ through their dependence on $\mathbf{H}$. If we define a detection factor, F as

$$F = \frac{\sigma_A^2 K}{2\sigma_w^2}, \tag{38}$$

then E and R can be rewritten as

$$E = \sigma_w^2 F \mathbf{H}^* \mathbf{Q}^{-1} \mathbf{H} \tag{39}$$

$$R = \sigma_w^2 F \mathbf{H}^* \mathbf{Q}^{-1} \mathbf{P}. \tag{40}$$

If R is expressed in polar notation as $R = |R| e^{i\theta_R}$, Eq. 35 can be written in terms of real variables as

$$\Lambda(\mathbf{S}, \mathbf{\Phi}, \mathbf{\Psi}, \mathbf{r}) = -\frac{A^2}{2\sigma_A^2} E + \frac{\sqrt{2}A}{\sigma_A} |R| \cos(\theta + \theta_R) \tag{41}$$

It is assumed that $\mathbf{\Phi}$ and $\mathbf{\Psi}$ are statistically independent; the values of amplitude and phase of the acoustic source have no dependence on parameters describing the environment. Furthermore, the amplitude is statistically

independent of the phase, and both amplitude and phase are statistically independent of source position. These assumptions allow the probability density function in Eq. 12 to be written as

$$p_{\mathbf{\Phi},\mathbf{\Psi}|\mathbf{S}}(\mathbf{\Phi},\mathbf{\Psi}|\mathbf{S}) = p_A(A)p_\theta(\theta)p_{\mathbf{\Psi}|\mathbf{S}}(\mathbf{\Psi}|\mathbf{S}). \tag{42}$$

Thus the OUFP equation becomes

$$p_{\mathbf{S}|\mathbf{r}}(\mathbf{S}|\mathbf{r}) = C(\mathbf{r})p_{\mathbf{S}}(\mathbf{S}) \int_{\mathbf{\Psi}} \Pi(\mathbf{S},\mathbf{\Psi},\mathbf{r})p_{\mathbf{\Psi}|\mathbf{S}}(\mathbf{\Psi}|\mathbf{S})\, d\mathbf{\Psi}, \tag{43}$$

where

$$\Pi(\mathbf{S},\mathbf{\Psi},\mathbf{r}) = \int_A \int_\theta \exp\left(\Lambda(\mathbf{S},\mathbf{\Psi},\theta,A,\mathbf{r})\right) p_A(A)p_\theta(\theta)\, d\theta\, dA \tag{44}$$

Maximum uncertainty is assumed about the transmitted phase, i.e., it is described by the following probability density function,

$$p_\theta(\theta) \;=\; \tfrac{1}{2\pi} \quad 0 \le \theta < 2\pi. \tag{45}$$

From reference [7, Eq. 3.915.4] we have

$$\frac{1}{2\pi}\int_0^{2\pi} \exp\left(\beta\cos(x+\theta)\right)\, dx = I_0(\beta), \tag{46}$$

where $I_0(\beta)$ is a modified Bessel function of order zero. Using this equation and Eqs. 41 and 45 in Eq. 44 gives

$$\Pi(\mathbf{S},\mathbf{\Psi},\mathbf{r}) = \int_A \exp\left(-\frac{A^2}{2\sigma_A^2}E\right) I_0\left(\frac{\sqrt{2}A}{\sigma_A}|R|\right) p_A(A)\, dA. \tag{47}$$

If the amplitude is assumed to be Rayleigh distributed with pdf

$$p_A(A) \;=\; \tfrac{A}{\sigma_A^2}\exp\left(-\tfrac{A^2}{2\sigma_A^2}\right) \quad A > 0, \tag{48}$$

a closed form expression for Eq. 47 is given in reference [4, page 311]:

$$\Pi(\mathbf{S},\mathbf{\Psi},\mathbf{r}) = (E+1)^{-1}\exp\left(\frac{|R|^2}{E+1}\right). \tag{49}$$

Collecting everything together, the OUFP equation for the narrowband signal in Gaussian noise problem is

$$p_{\mathbf{S}|\mathbf{r}}(\mathbf{S}|\mathbf{r}) = C(\mathbf{r})p_{\mathbf{S}}(\mathbf{S}) \int_{\mathbf{\Psi}} (E+1)^{-1} \exp\left(\frac{|R|^2}{E+1}\right) p_{\mathbf{\Psi}|\mathbf{S}}(\mathbf{\Psi}|\mathbf{S})\, d\mathbf{\Psi}, \qquad (50)$$

where

$$E = \sigma_w^2 F \mathbf{H}^* \mathbf{Q}^{-1} \mathbf{H} \qquad (51)$$

$$R = \sigma_w^2 F \mathbf{H}^* \mathbf{Q}^{-1} \mathbf{P}. \qquad (52)$$

4.4 Matched Field Processing

If the acoustic environmental parameters are known, the optimum uncertain field processor reduces to

$$p_{\mathbf{S}|\mathbf{r}}(\mathbf{S}|\mathbf{r}) = C(\mathbf{r})p_{\mathbf{S}}(\mathbf{S})(E+1)^{-1} \exp\left(\frac{|R|^2}{E+1}\right), \qquad (53)$$

where E and R are now calculated only for the known environment. This is the optimum algorithm for locating a narrowband source in a known environment and the implementation of this equation is termed the optimum matched field processor (OMFP).

It is instructive to consider maximum a posteriori (MAP) estimation of the source position. MAP estimates are obtained by determining the peak of $p_{\mathbf{S}|\mathbf{r}}(\mathbf{S}|\mathbf{r})$. Equivalently, we can determine the peak of any monotonic function of $p_{\mathbf{S}|\mathbf{r}}(\mathbf{S}|\mathbf{r})$. A particularly illuminating monotonic function is

$$f(\mathbf{S}) = \frac{1}{F} \ln\left(p_{\mathbf{S}|\mathbf{r}}(\mathbf{S}|\mathbf{r})/C(\mathbf{r})\right). \qquad (54)$$

Substituting from Eq. 53 gives

$$f(\mathbf{S}) = \frac{|R|^2}{F(E+1)} - \frac{1}{F}\ln(E+1) + \frac{1}{F}\ln(p_{\mathbf{S}}(\mathbf{S})). \qquad (55)$$

Using the definitions of R and E, and assuming that $E \gg 1$, yields

$$f(\mathbf{S}) = \sigma_w^2 \frac{|\mathbf{H}^*\mathbf{Q}^{-1}\mathbf{P}|^2}{\mathbf{H}^*\mathbf{Q}^{-1}\mathbf{H}} - \frac{1}{F}\ln(\mathbf{H}^*\mathbf{Q}^{-1}\mathbf{H}) + \frac{1}{F}\ln(p_{\mathbf{S}}(\mathbf{S})). \qquad (56)$$

For high values of the detection factor this can be approximated as

$$f(\mathbf{S}) = \sigma_w^2 \frac{|\mathbf{H}^* \mathbf{Q}^{-1} \mathbf{P}|^2}{\mathbf{H}^* \mathbf{Q}^{-1} \mathbf{H}}. \tag{57}$$

and if the noise is spatially uncorrelated this reduces further to

$$f(\mathbf{S}) = \frac{|\mathbf{H}^* \mathbf{P}|^2}{\mathbf{H}^* \mathbf{H}}. \tag{58}$$

This equation was first suggested for use in matched field localization in reference [6]. It is a generalization of the conventional (Bartlett) beamformer. (In conventional beamforming $\mathbf{H}$ corresponds to the steering vector for a plane-wave arrival.) The surface obtained by plotting $f(\mathbf{S})$ as a function of $\mathbf{S}$ for a particular (usually noise free) observation, $\mathbf{P}$, is known as an *ambiguity surface.*

4.5 Acoustic Tomography

The source position a posteriori probability density function can also be written as

$$p_{\mathbf{S}|\mathbf{r}}(\mathbf{S}|\mathbf{r}) = \int_{\mathbf{\Psi}} p_{\mathbf{S},\mathbf{\Psi}}(\mathbf{S}, \mathbf{\Psi}|\mathbf{r})\, d\mathbf{\Psi}. \tag{59}$$

That is, the OUFP equation is a marginal density function computed from the joint probability density function of $\mathbf{S}$ (the set of source position coordinates) and $\mathbf{\Psi}$ (the set of environment parameters).

From equation 50 the joint pdf can be identified as

$$p_{\mathbf{S},\mathbf{\Psi}}(\mathbf{S}, \mathbf{\Psi}|\mathbf{r}) = C(\mathbf{r}) p_{\mathbf{S}}(\mathbf{S}) p_{\mathbf{\Psi}}(\mathbf{\Psi})(E+1)^{-1} \exp\left(\frac{|R|^2}{E+1}\right). \tag{60}$$

($\mathbf{S}$ and $\mathbf{\Psi}$ are assumed to be statistically independent.) $p_{\mathbf{S}}(\mathbf{S})$ and $p_{\mathbf{\Psi}}(\mathbf{\Psi})$ are the a priori probability density functions. Recall that E and R are dependent on $\mathbf{S}$ and $\mathbf{\Psi}$ through their dependence on the acoustic transfer function, $\mathbf{H}$.

It has been shown that, if $\mathbf{\Psi}$ is known, this equation reduces to the optimum matched field equation. If there is uncertainty in $\mathbf{\Psi}$ then computing the marginal density over $\mathbf{\Psi}$ results in the optimum uncertain field processor. Other situations are worthy of mention. If the source position is known, or the marginal over the source position is calculated, then the joint pdf

reduces to an a posteriori pdf describing the environment parameters, Ψ. The pdf can be used to estimate the values of the environment parameters. From these estimates a "picture" of the acoustic sound speed field can be obtained. This represents one approach to the *acoustic ocean tomography* problem. Another concept suggested by the previous equation is that of simultaneous localization and tomography. Some examples of this are given in the results.

5 Results-Sensitivity to Large Scale Range Independent Perturbations

In this section, localization processor sensitivity to uncertainty in the major parameters of the deep-ocean sound velocity profile is investigated by Richardson [10, 11]. A subsection on acoustic tomographic estimation of sound velocity profile parameters is also included.

A range-independent acoustic environment is simulated and the normal mode acoustic propagation model is used.

5.1 The Sound Velocity Profile Model

The sound velocity profile is modeled as

$$c(z) = c_M(z) + w_1 e_1(z) + w_2 e_2(z), \tag{61}$$

where $c_M(z)$ is a Munk profile with parameters c_0 (axis sound speed) equal to 1500 m/s and z_0 (axis depth) equal to 1000 m. $e_1(z)$ and $e_2(z)$ are orthogonal perturbation functions. We will investigate the performance sensitivity of two localization processors with respect to uncertainty in the weight parameters w_1 and w_2.

The functions $e_1(z)$ and $e_2(z)$ were calculated from a Gram-Schmidt orthogonalization [5] on the function set $\{f_1(z), f_2(z)\}$, where

$$f_1(z) = c_1(z) - c_M(z) \tag{62}$$

$$f_2(z) = c_2(z) - c_M(z). \tag{63}$$

$c_1(z)$ and $c_2(z)$ are Munk profiles with parameters, $c_0 = 1510$ m/s (axis speed), $z_0 = 1000$ m (axis depth) and $c_0 = 1500$ m/s, $z_0 = 950$ m respectively. $c_1(z)$ differs from $c_M(z)$ only in the value of the c_0 parameter, while $c_2(z)$ differs from $c_M(z)$ only in the value of the z_0 parameter.

The profile $c_M(z)$ is plotted in the center graph in Fig. 1. The other graphs in the figure are plots of $\Delta(z) = w_1 e_1(z) + w_2 e_2(z)$ for different values of w_1 and w_2. A value of w_1 other than zero essentially adds a constant value to $c_M(z)$ for all depths. Values of w_2 different from zero affect only the portion of the SVP above the channel axis and can be used to raise or lower the depth of the sound speed axis.

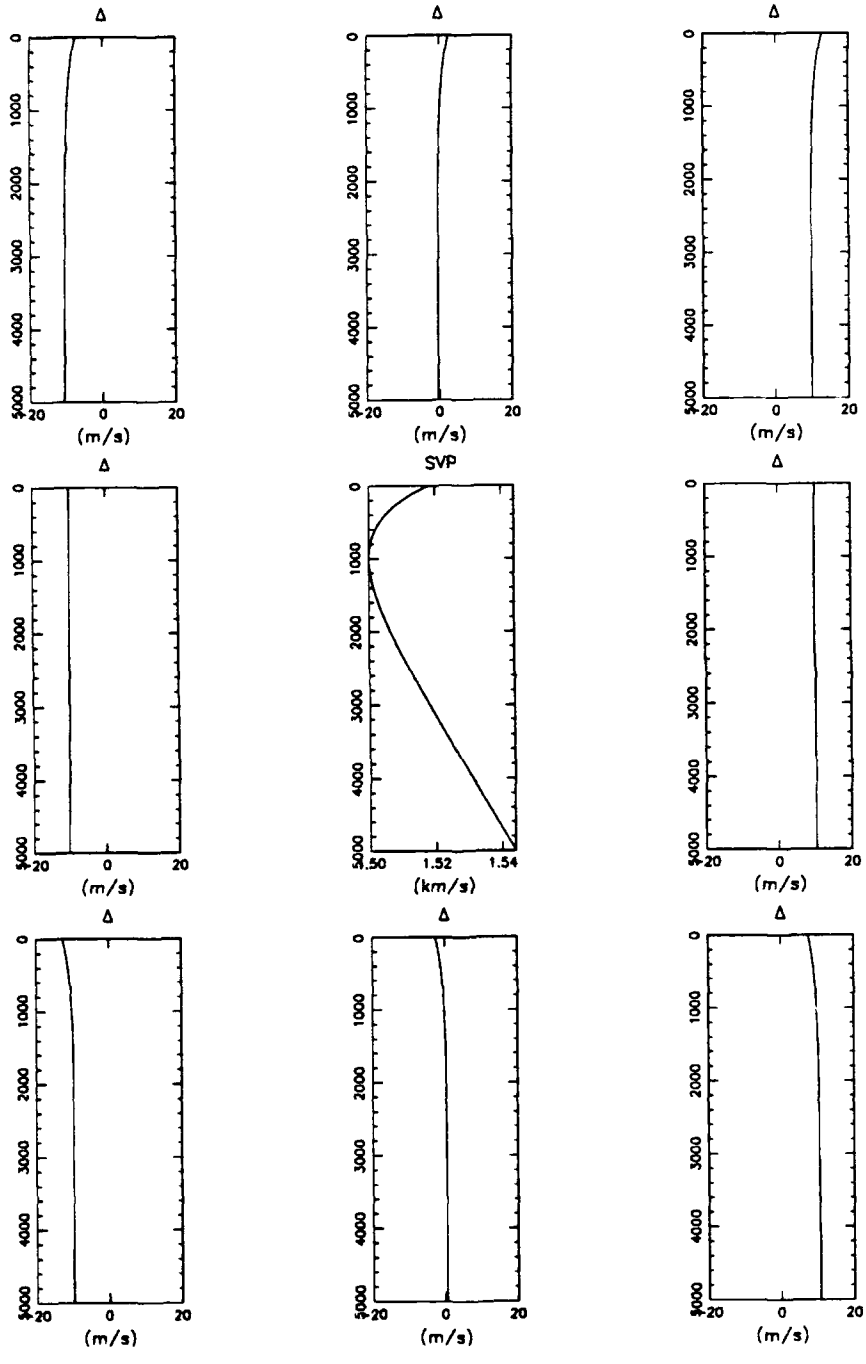

Figure 1: Nominal Munk profile (center graph) and Delta profiles for different values of w_1 and w_2. Values for each Delta profile are (clockwise from upper left): $w_1 = -1$, $w_2 = -1$; $w_1 = 0$, $w_2 = -1$; $w_1 = 1$, $w_2 = -1$; $w_1 = 1$, $w_2 = 0$; $w_1 = 1$, $w_2 = 1$; $w_1 = 0$, $w_2 = 1$; $w_1 = -1$, $w_2 = 1$; $w_1 = -1$, $w_2 = 0$

5.2 Estimation Sensitivity

The performance of the optimum uncertain field processor (OUFP) and that of the optimum matched field processor (OMFP) are examined in the presence of sound velocity profile uncertainty.

Since the optimum matched field processor is not the optimum localization processor to use in an uncertain environment, the terminology is a little confusing. The word "optimum", in the label "optimum matched field processor", is now being used to identify a particular matched field processor and not as an indication of level of performance. To remedy the problem, the notation mismatched-OMFP will be used to indicate the optimum matched field processor when operating in an uncertain environment.

5.2.1 Range/Depth Estimation

In the simulated results presented in this section the acoustic source is at a depth of 1000 m and at a range of 50000 m from the receive array. A vertical array of 10 elements, with the shallowest element at 200 m and the elements spaced 200 m apart, is used. The transmitted frequency is 15 Hz. The detection factor is 92 dB.

The mismatched-OMFP calculates replica fields assuming that w_1 and w_2 are both zero. (It is matched to only the environment characterized by those values.)

The OUFP assumes that w_1 is uniformly distributed between the values -0.2 and 0.2 and that w_2 is equal to zero.

We investigate processor performance by computing and plotting the a posteriori source position probabilities. Each point in the a posteriori probability graphs represents the probability that the acoustic source is located within a 5 meter depth bin and a 1000 meter range bin.

The output of the mismatched-OMFP for an actual environment that is characterized by values of w_1 and w_2 both equal to zero is shown is shown in Fig. 2. This is the environment for which the processor is designed. It does a good job of locating the source as evidenced by the small cluster of peaks near the true source position.

The output of the OMFP for the same environment is shown in Figure 3. The observation (signal and noise) is the same as that for the mismatched-OMFP of the previous figure. The two processors do, of course, process

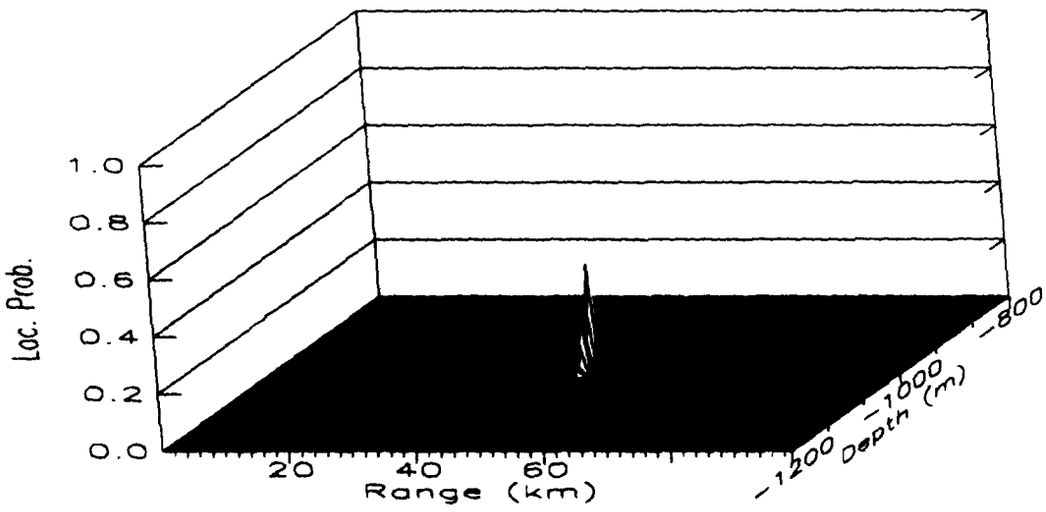

Figure 2: Mismatched-OMFP a posteriori range-depth pdf output for the environment characterized by values of w_1 and w_2 both equal to zero.

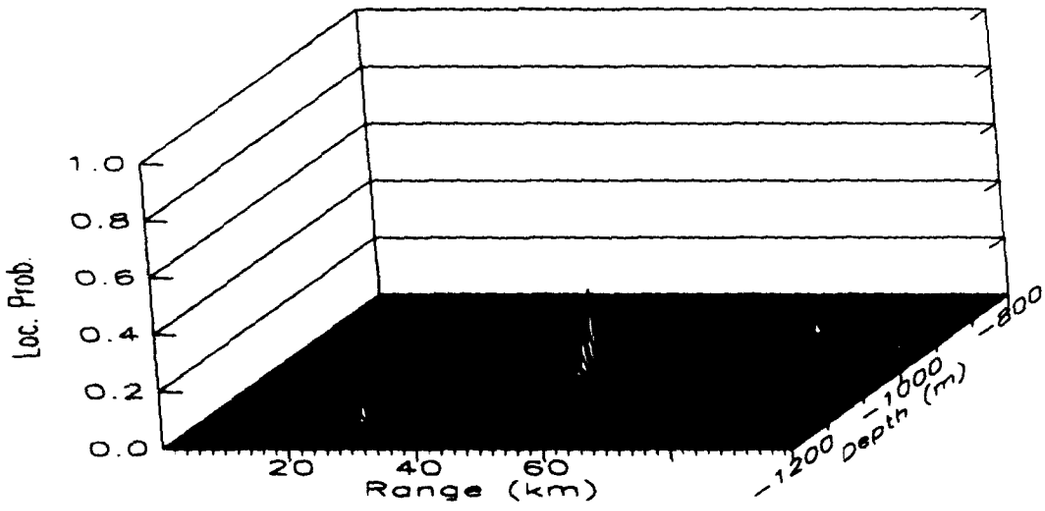

Figure 3: OUFP a posteriori range-depth pdf output for the environment characterized by values of w_1 and w_2 both equal to zero.

the observation differently. The OUFP also does a good job of locating the source; however, the main peak is slightly lower than that in the previous figure and some small spurious peaks at a distance away from the source. This can be explained by the fact that the OUFP is looking over a larger set of possible environments than the mismatched-OMFP and there is a corresponding penalty in performance. The OUFP may not be the best processor in any particular environment, but rather, it is the best processor over all possible uncertain environments.

The output of the mismatched-OMFP for an actual environment characterized by w_1 equal to 0.2 and w_2 equal to 0.0 is shown in Fig. 4. (This corresponds to a mismatch between the assumed and actual sound velocity profiles of approximately 2 m/s.) The processor is the same as that used in Fig. 2, but the observation is now different. The processor is mismatched to this environment and the localization performance is poor. There is no peak at the actual source position, although some small peaks appear nearby, and the largest peak is at a range of about 30000 m and a depth of 800 m.

The output of the OUFP for the same observation is shown in Fig. 5. The OUFP does a much better job of locating the source as indicated by the large peak at the true source position. (The fact that performance is better here than in Fig. 3 violates no principles. The processors are identical, but the observations are different.) This clearly illustrates the advantage of using an uncertain field processor in an uncertain environment.

5.2.2 Range Estimation

We now concentrate on the estimation of only one source position coordinate at a time. This allows us to examine the sensitivity of the localization processors to uncertainty in the environment in greater detail.

The range estimation problem is considered first. The source depth is known and equal to 1000 m. The localization scenario is the same as in the previous section, except that the detection factor has been reduced to 86 dB. (The higher detection factor is not necessary for estimation of a single source coordinate.) These simulations are noise-free. This prevents misinterpretation of spurious noise peaks. This could also be accomplished by looking at many noisy simulation runs, but this is prohibited by computer processing time requirements.

The localization processor output is now an a posteriori probability line

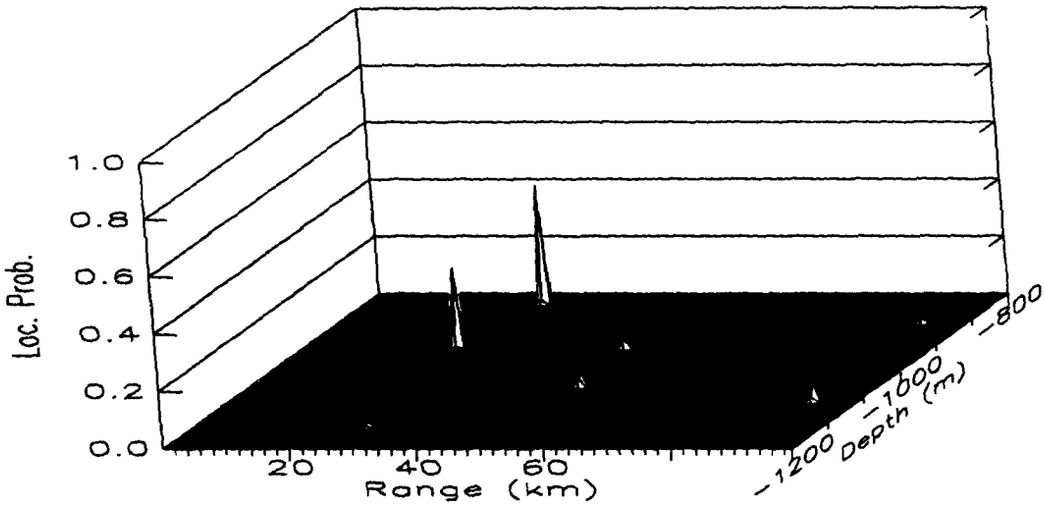

Figure 4: Mismatched-OMFP a posteriori range-depth pdf output for the environment characterized by values of w_1 equal to 0.2 and w_2 equal to 0.0.

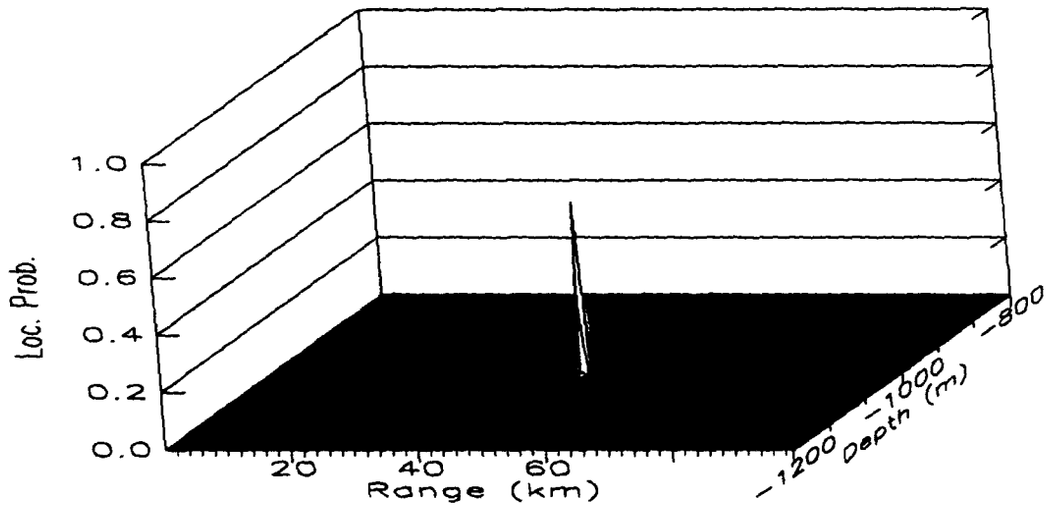

Figure 5: OUFP a posteriori range-depth pdf output for the environment characterized by values of w_1 equal to 0.2 and w_2 equal to 0.0.

instead of a surface as in the previous section. Multiple lines, corresponding to different actual environments, are displayed simultaneously in a three-dimensional graph. This allows us to visualize the change in processor performance with a change in environment. In an actual implementation of the localization processor only one line (the line corresponding to the actual environment) will be observed.

The range a posteriori pdf output of the mismatched-OMFP for different environment values of w_2 is shown in Fig. 6. The value of w_1 is zero. This processor is matched to an environment characterized by values of w_1 and w_2 equal to zero. The figure indicates that the performance of the processor is not sensitive to variation in w_2 between -1 and 1. (This corresponds to a variation in the depth of the sound axis of about 100 meters.)

The corresponding result for the OUFP is shown in Fig. 7. The OUFP assumes that the value of w_2 is uniformly distributed between -1 and 1. This processor is also not sensitive to the actual value of w_2.

The mismatched-OMFP output for different values of the environment parameter w_1 is shown in Fig. 8. The value of w_2 is zero. The processor is matched to an environment characterized by values of w_1 and w_2 equal to zero and there is a large peak at the true source range for the matched case (w_1 equal to zero). In the mismatched cases however, several spurious peaks start to appear at large distances from the true source position. There are cases in which mismatch is less than .1 (corresponding to knowledge of the SVP to within 1 m/s) and the largest peak occurs at a distance of greater than 10000 meters from the true source range.

The reduced sensitivity of the OUFP is illustrated in Figure 9. This processor assumes that the value of w_1 is uniformly distributed between -1 and 1. A distinctive ridge, extending across all values of w_1, is present at the true source range of 50000 m. Such ridges are characteristic of robust localization processors.

5.2.3 Depth Estimation

We now consider the problem of estimating the acoustic source depth when the range to the source (50000 m) is known.

The output of the mismatched-OMFP as a function of the parameter w_2 is shown in Fig. 10. The mismatched-OMFP assumes the environment is known and is characterized by values of w_1 and w_2 equal to zero. The

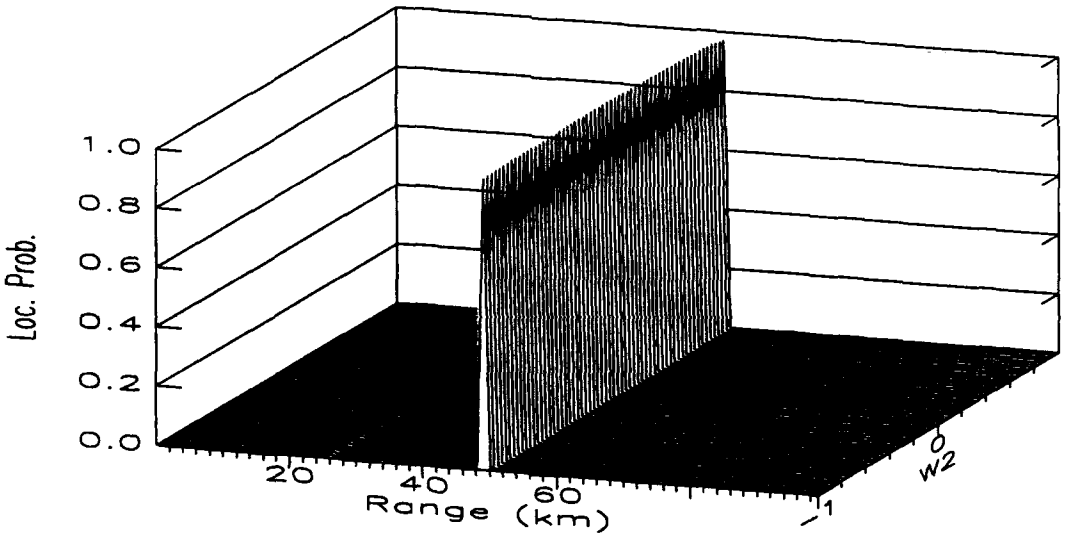

Figure 6: Mismatched-OMFP a posteriori range pdf output as a function of the value of w_2. w_1 is equal to zero.

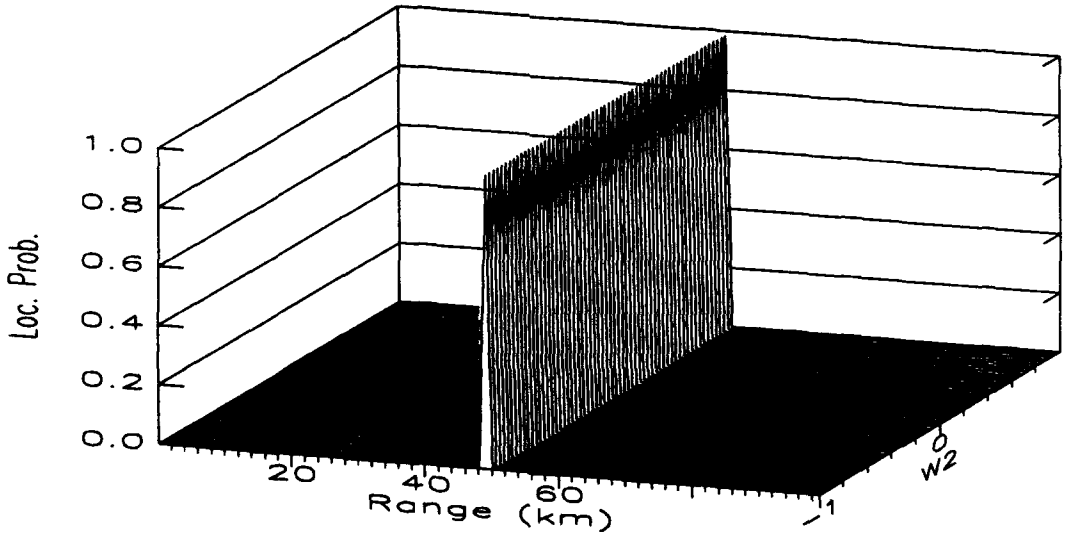

Figure 7: OUFP a posteriori range pdf output as a function of the value of w_2. w_1 is equal to zero.

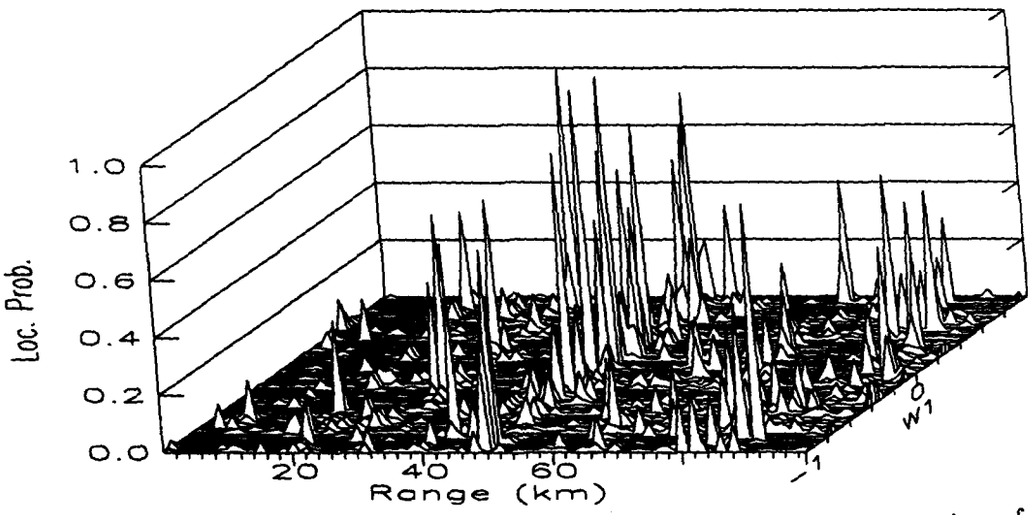

Figure 8: Mismatched-OMFP a posteriori range pdf output as a function of the value of w_1. w_2 is equal to zero.

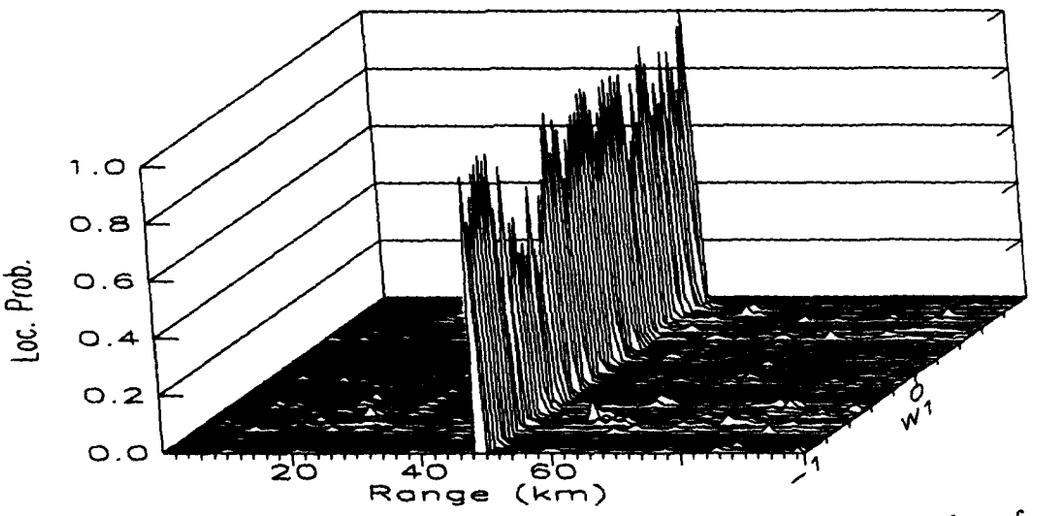

Figure 9: OUFP a posteriori range pdf output as a function of the value of w_1. w_2 is equal to zero.

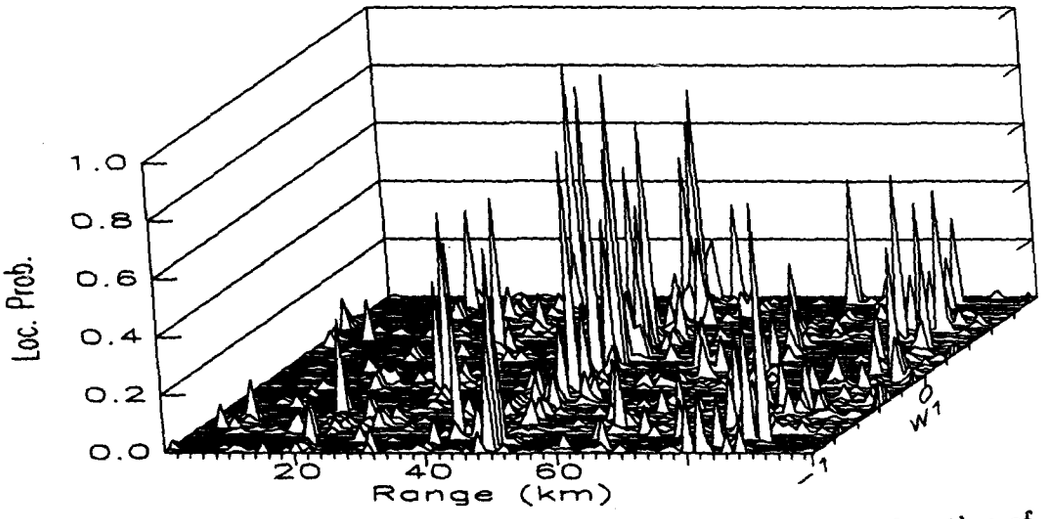

Figure 8: Mismatched-OMFP a posteriori range pdf output as a function of the value of w_1. w_2 is equal to zero.

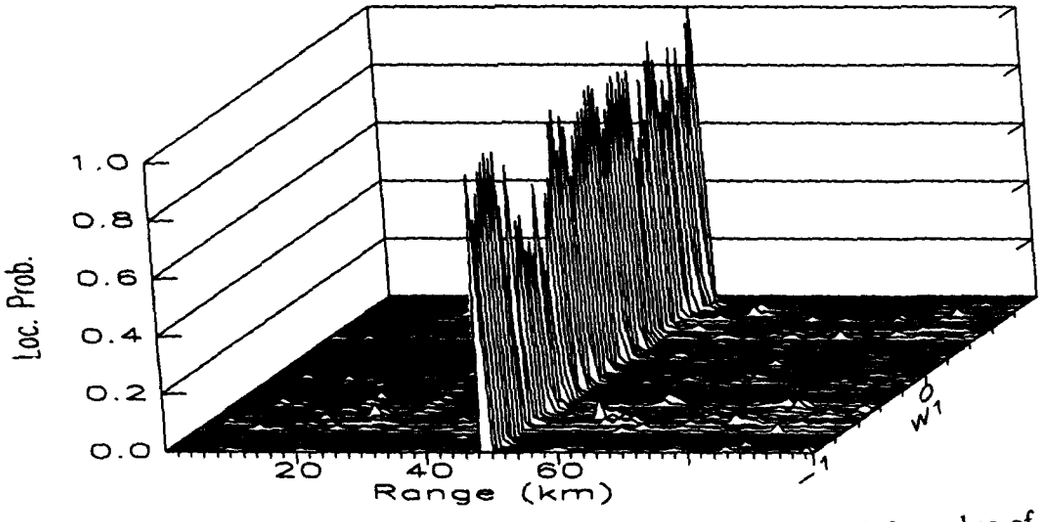

Figure 9: OUFP a posteriori range pdf output as a function of the value of w_1. w_2 is equal to zero.

result indicates that depth estimation by the mismatched-OMFP, like range estimation, is not sensitive to uncertainty in w_2.

The corresponding output of the optimum uncertain field processor is shown in Fig. 11. Depth estimation by the OUFP is also not sensitive to uncertainty in w_2. The height of the ridge is just slightly less than that in the previous figure.

The output of the mismatched-OMFP for different values of w_1 is shown in Fig. 12. There is a cluster of peaks at the true source depth in the region where w_1 is equal to zero. For values of w_1 away from zero spurious peaks appear at depths different than the true depth.

The OUFP output is shown in Fig. 13. A ridge at the true source depth, indicating the robustness of the OUFP when operating in an uncertain environment, is clearly observed.

5.3 Acoustic Tomography

As discussed in Chapter 4, a processor which can simultaneously be used to locate a source and estimate the acoustic environment parameters can be constructed based on Eq. 60. Simulation results for this problem are presented in this section.

The source position and receiver geometry are the same as in the previous section. The source acoustic frequency is 15 Hz. The source detection factor is 86 dB.

Simultaneous estimation of one source position coordinate and the environment parameter w_1 is considered first. The other position coordinate and w_2 are known.

The localization/tomography processor output when the source range and the value of w_1 are unknown is shown in Fig. 14. (Recall that the processor output is the joint range and w_1 pdf.) The graph indicates that there is a high probability that the source is located at a range of 50000 m and that the value w_1 is equal to zero. Since this corresponds to the true values of these parameters, it can be concluded that the processor has done a good job in this case.

The joint depth and w_1 pdf is shown in Fig. 15. The processor also does a good job of estimating both source depth and w_1. The figure indicates a that there is a high probability of locating the source at a depth of 1000 m

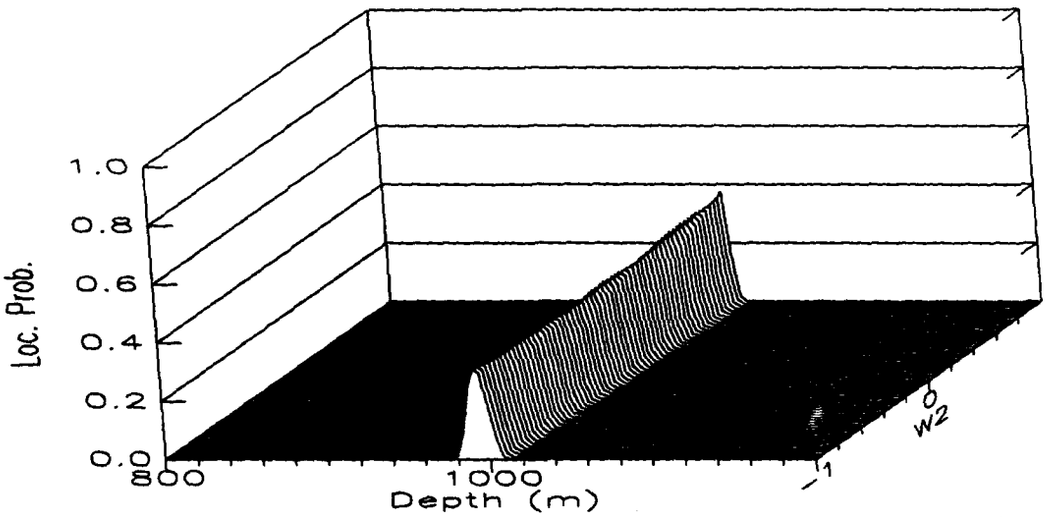

Figure 10: Mismatched-OMFP a posteriori depth pdf output as a function of the value of w_2. w_1 is equal to zero.

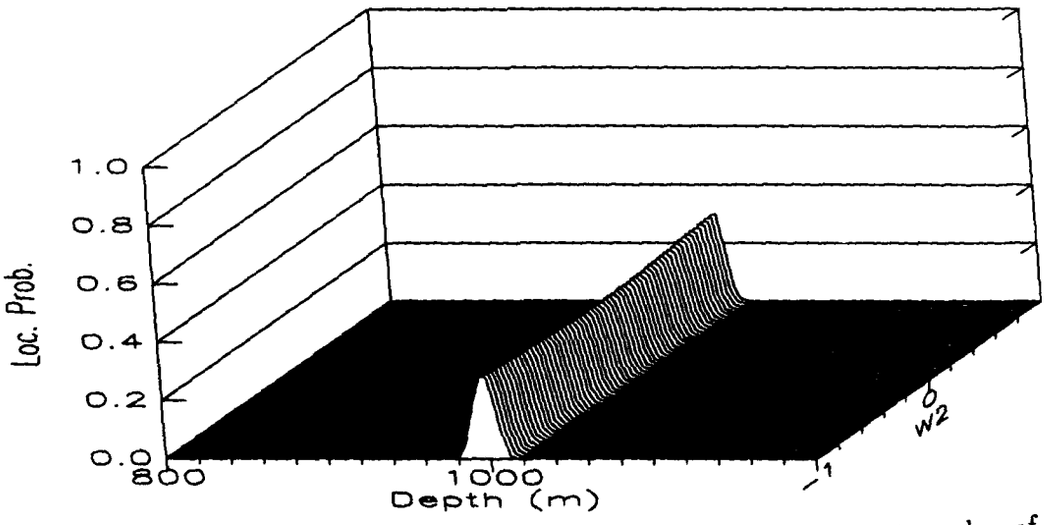

Figure 11: OUFP a posteriori depth pdf output as a function of the value of w_2. w_1 is equal to zero.

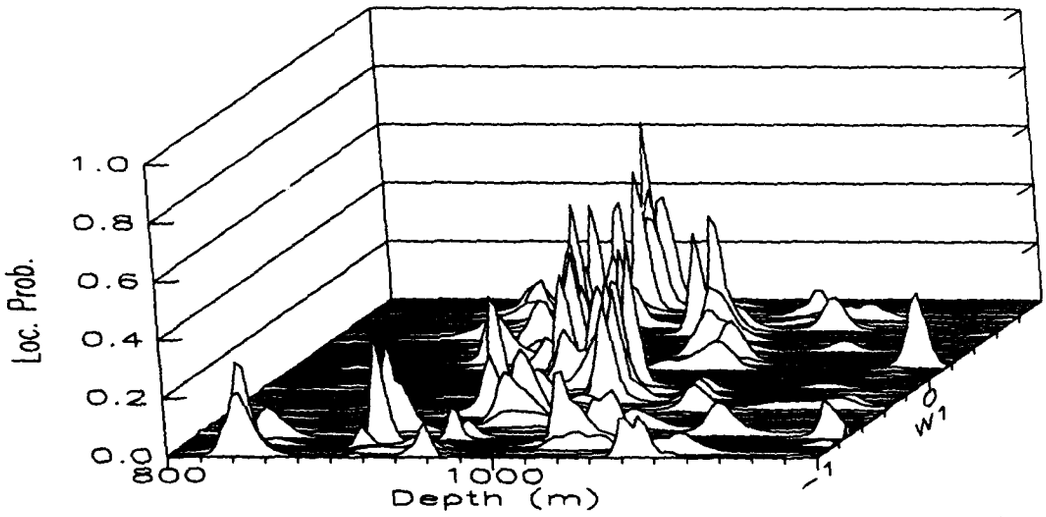

Figure 12: Mismatched-OMFP a posteriori depth pdf output as a function of the value of w_1. w_2 is equal to zero.

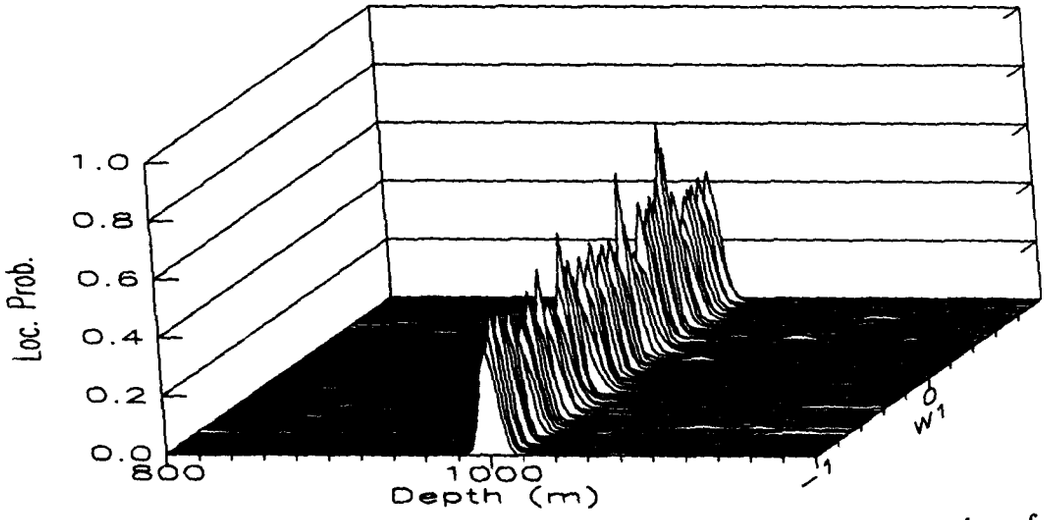

Figure 13: OUFP a posteriori depth pdf output as a function of the value of w_1. w_2 is equal to zero.

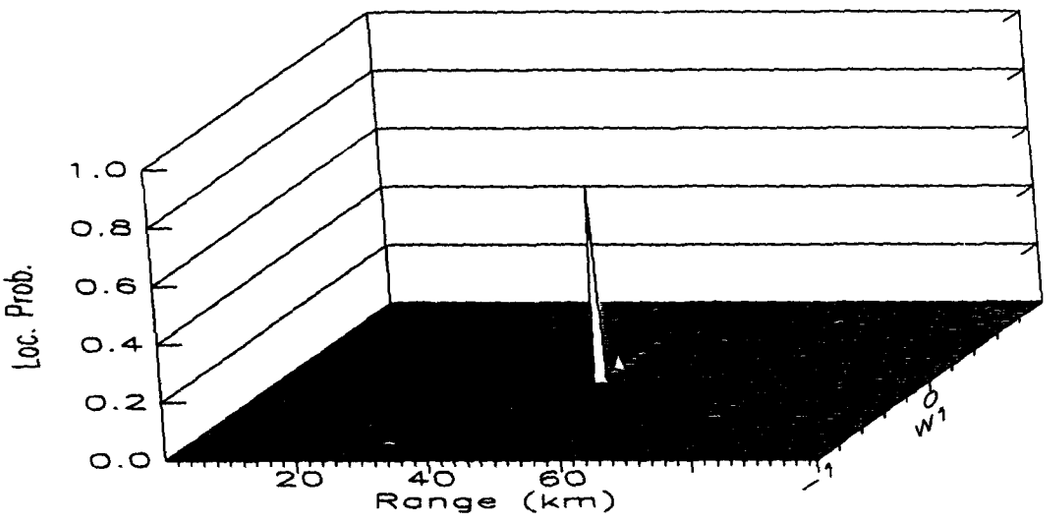

Figure 14: Localization/tomography processor joint range and w_1 pdf output. The depth and w_2 are known.

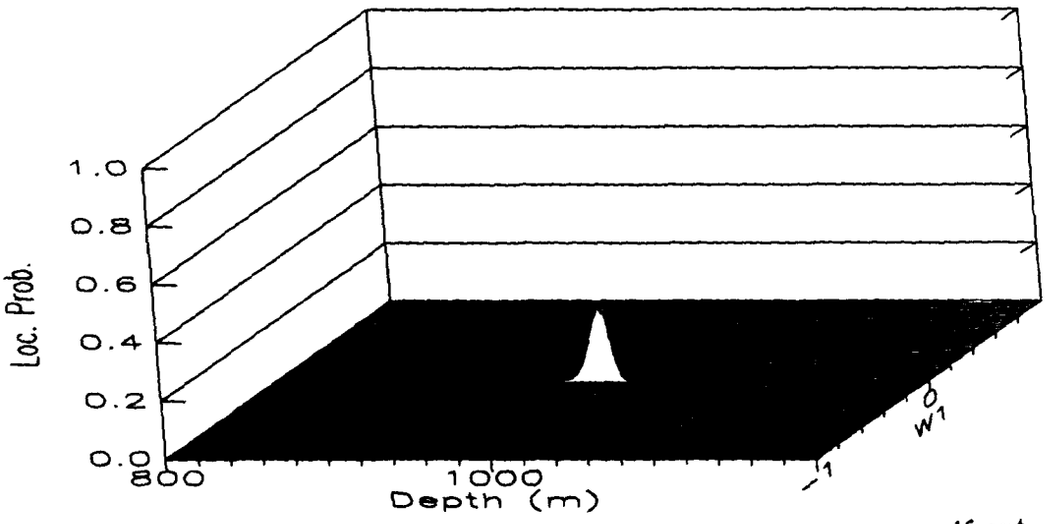

Figure 15: Localization/tomography processor joint depth and w_1 pdf output. The range and w_2 are known.

and that the value of w_1 is zero. These are the correct values of these two parameters.

These results help to explain why the mismatched-OMFP is sensitive to uncertainty in w_1 while the OUFP is not. Considering only range estimation for a moment and referring to Fig. 14, the output of the mismatched-OMFP will be the same as the line in the figure with a value of w_1 that corresponds to the actual value of w_1. For example, if the processor is matched to a value of w_1 equal to zero, the processor output will be the $w_1 = 0$ line in the figure. A very good estimate of range is then obtained. If, however, the processor is mismatched to some other value of w_1, then a distinctive peak at the true source range is not seen in the corresponding line in the figure and the processor performance is then poor. On the other hand, the OUFP averages across the lines and finds a line with a high peak at the true range. (The line corresponding to the actual value of w_1.) This implies the OUFP output will also have a peak at the true source range. Similar comments apply to the depth localization cases.

The joint range and w_2 pdf is shown in Fig. 16. A ridge appears at the true range, but no easily identifiable peak appears in the ridge. This means that good range estimation is possible, but good estimates of w_2 are not obtainable. This is predictable from the mismatched-OMFP results. The mismatched-OMFP range estimates are not sensitive to uncertainty in w_2, which implies the joint range and w_2 pdf has a ridge across all values of w_2. This makes estimation of w_2 difficult.

The joint depth and w_2 pdf is shown in Fig. 17. There is a small ridge at the true source depth but it is quite difficult to see in the graph. The low ridge height indicates difficulty when trying to estimate depth and w_2 simultaneously.

Of course, the performance is a function of the signal-to-noise ratio (detection factor). Figs. 18 and 19 are the same as the two previous figures except the detection factor has been raised by 14 dB. Since there is a peak in the joint range or depth and w_2 pdf at this signal-to-noise ratio, good estimates should be obtained. Since the mismatched-OMFP corresponds to a single line in these figures, this processor will be sensitive to uncertainty in w_2 at this signal-to-noise ratio.

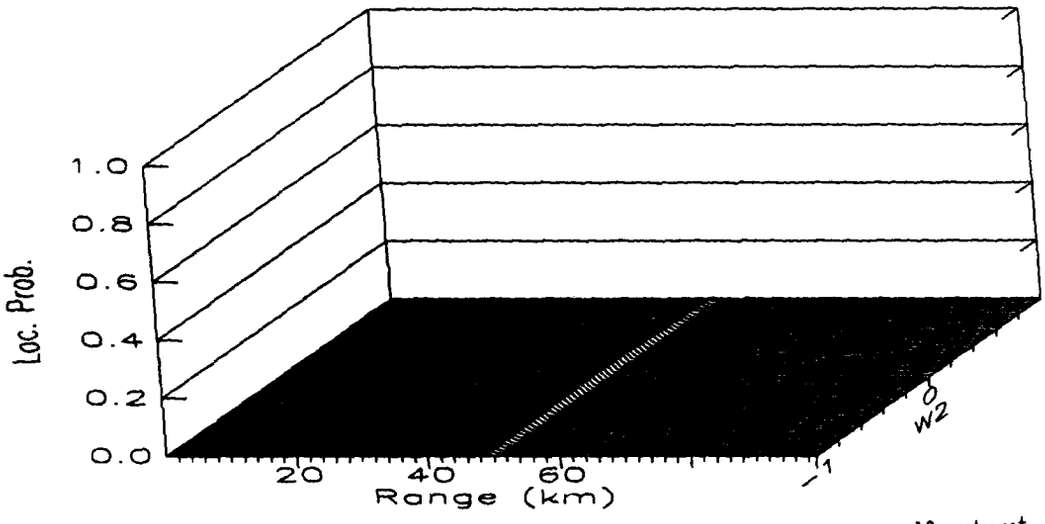

Figure 16: Localization/tomography processor joint range and w_2 pdf output. The depth and w_1 are known.

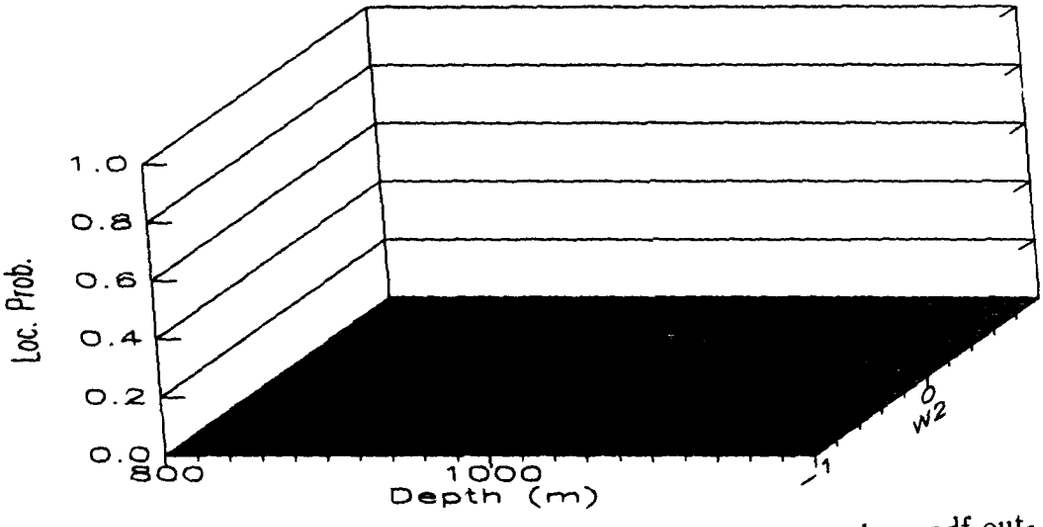

Figure 17: Localization/tomography processor joint depth and w_2 pdf output. The range and w_1 are known.

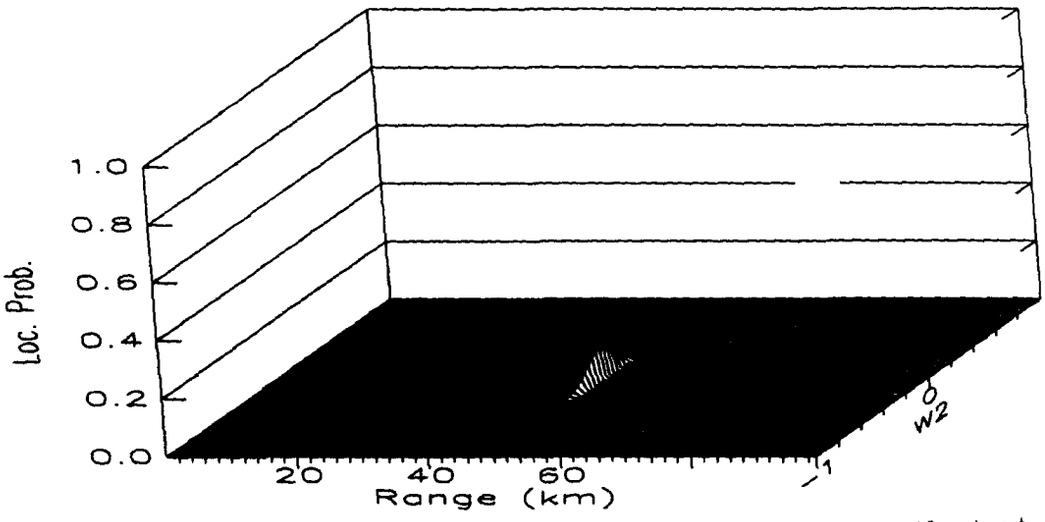

Figure 18: Localization/tomography processor joint range and w_2 pdf output. The depth and w_1 are known. The detection factor has been increased by 14 dB.

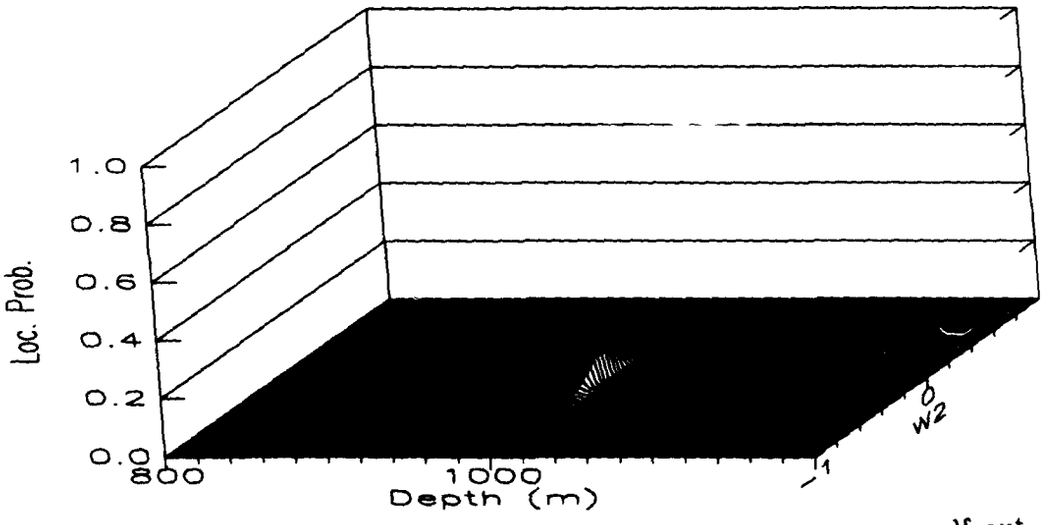

Figure 19: Localization/tomography processor joint depth and w_2 pdf output. The range and w_1 are known. The detection factor has been increased by 14 dB.

5.4 Summary

The degradation in performance that can occur when a matched field processor is used in an environment for which it has not been designed has been illustrated. In an uncertain environment the performance of the matched field processor may be extremely poor. On the other hand, the optimum uncertain field processor is robust in an uncertain environment. A properly designed uncertain field processor can achieve good performance regardless of the actual acoustic environment.

6 Results-Sensitivity to Small Scale Range Independent Perturbations

In the previous section we showed that the OUFP is less sensitive to uncertainty in the major parameters of the SVP than a matched field processor. The assumed profile uncertainty is not actually typical of that of the real ocean. In this section sensitivity with respect to perturbations in the SVP on the order of those which might occur in the surface layer is investigated by Richardson [10, 11].

6.1 The Sound Velocity Profile Model

The sound velocity profile is modeled as

$$c(z) = c_M(z) + c_p \exp\left(-z^2/2\sigma_p^2\right) \tag{64}$$

where $c_M(z)$ is a Munk profile with parameters c_0 (axis sound speed) equal to 1500 m/s and z_0 (axis depth) equal to 1000 m. (This is the typical profile shown in the introductory section.) The second term represents a Gaussian perturbation in the SVP that occurs at the water surface. For the results presented in this section, the perturbation standard deviation width is 20 m. The localization sensitivity with respect to the height of the perturbation, c_p, is investigated.

Urick [14] shows several temperature profiles of the surface layer as measured near Bermuda over a 24 hour period. The profiles vary by about 5°C during this time period. (Cooling occurs at night with warming taking place during the day.) This corresponds to a variation in sound speed of approximately 8 m/s. We investigation variations of this order of magnitude.

6.2 Estimation Sensitivity

As in the previous section, the range to the source is 50000 meters. A 10 element array, with elements 200 m apart, is used. The detection factor is 86 dB. The normal mode acoustic model is used to calculate the observation and the replica fields.

A shallower source depth is used and we look at localization performance as a function of source depth and frequency.

6.2.1 Range Estimation

For the first set of results the source is at a depth of 15 m and is operating at a frequency of 15 Hz. The mismatched-OMFP range estimation sensitivity to uncertainty in c_p is shown in Fig. 20. (The c_p axis is labeled Delta in the figure.) The mismatched-OMFP is matched to a perturbation height of zero. The processor shows very little sensitivity to perturbation height uncertainty over the range of mismatch examined.

The corresponding OUFP output is shown in Fig. 21. This OUFP assumes uncertainty in the surface layer and that the perturbation amplitude is uniformly distributed between -10 and 10 m/s. The high ridge indicates that this processor is also not sensitive to uncertainty in the perturbation amplitude.

The insensitivity is due to the large ratio of wavelength to perturbation width. At 15 Hz, the acoustic wavelength is approximately 100 m. This is five times larger than the standard deviation width of the perturbation. Figs. 22 and 23 show the mismatched-OMFP and OUFP output for an acoustic source operating at 60 Hz. The wavelength at this frequency is approximately 25 m, which is about equal to the perturbation width. At this higher frequency the mismatched-OMFP is quite sensitive to mismatch greater than about 2.5 m/s. On the other hand, the OUFP performs robustly with respect to uncertainty in the actual value of c_p.

The sensitivity of matched field processing is a function not only of frequency, but source depth as well. Figs. 24 and 25 correspond to Fig. 22 except the source depths are 30 and 60 m. At 30 m the mismatched-OMFP is still somewhat sensitive to c_p uncertainty. At 60 m the mismatched-OMFP output is relatively insensitive to uncertainty in c_p. At this depth the source is well below the surface layer perturbation and the resulting acoustic field is relatively unaffected by it.

6.2.2 Depth Estimation

We now look at depth estimation performance when the range to the source is known (50000 m). The source is at a depth of 15 m for all of the results in this section.

Fig. 26 shows the sensitivity of the mismatched-OMFP to mismatch in perturbation height for the 15 Hertz source. The peak is in approximately

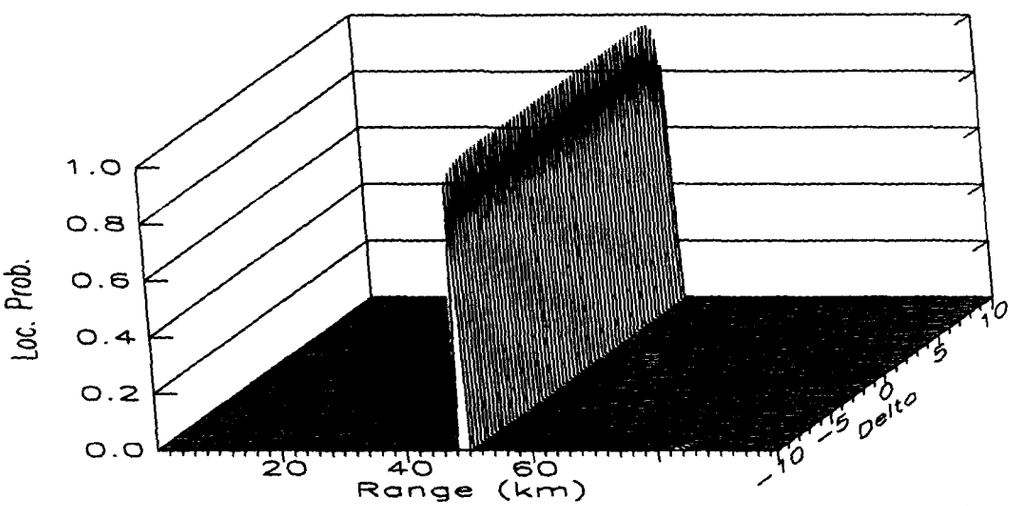

Figure 20: Mismatched-OMFP a posteriori range pdf output as a function of perturbation amplitude. The true source range is 50000 m. The source depth is 15 m and the frequency is 15 Hz.

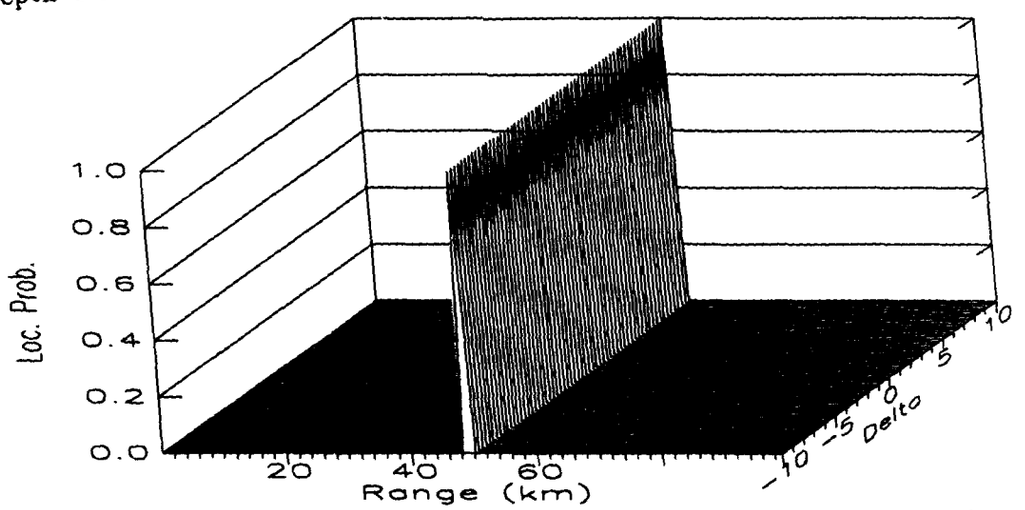

Figure 21: OUFP a posteriori range pdf output as a function of perturbation amplitude. The true source range is 50000 m. The source depth is 15 m and the frequency is 15 Hz.

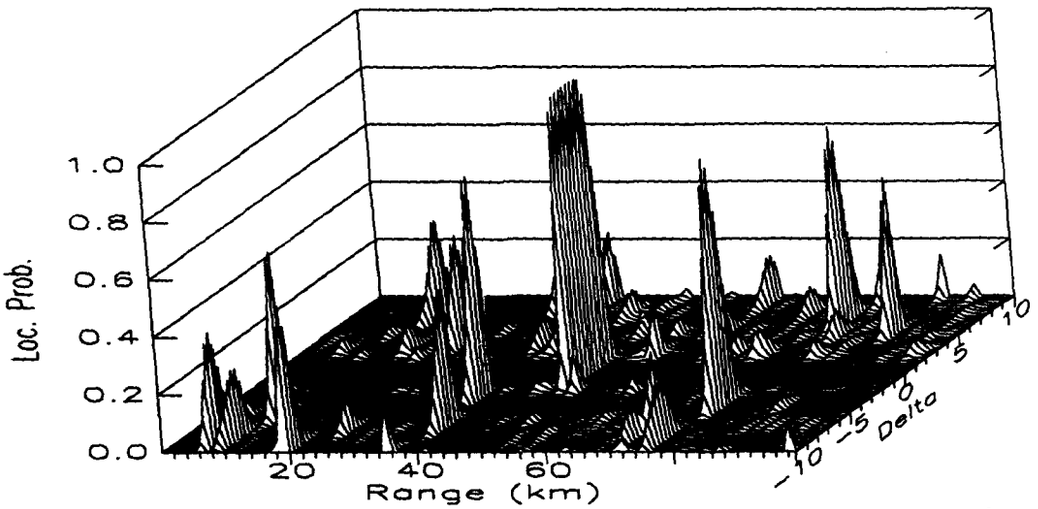

Figure 22: Mismatched-OMFP a posteriori range pdf output as a function of perturbation amplitude. The true source range is 50000 m. The source depth is 15 m and the frequency is 60 Hz.

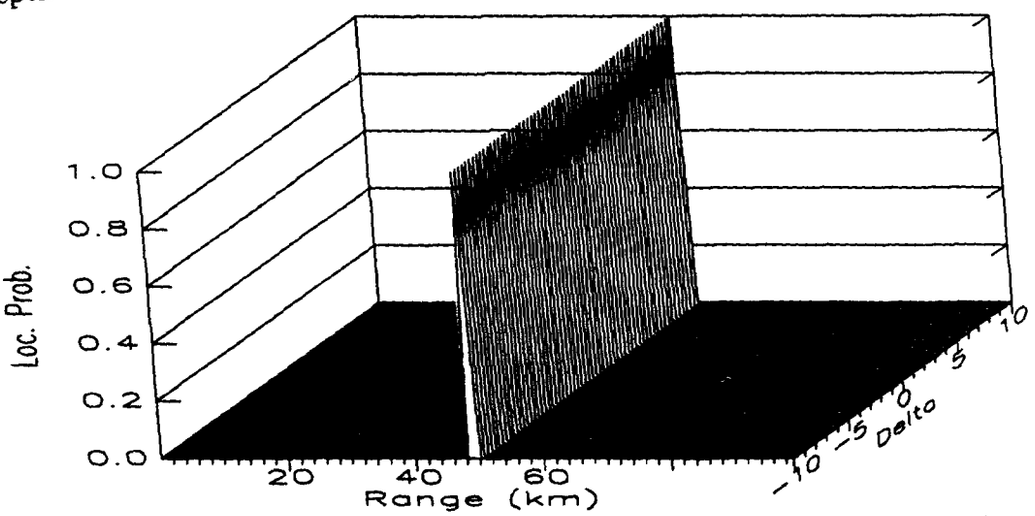

Figure 23: OUFP a posteriori range pdf output as a function of perturbation amplitude. The true source range is 50000 m. The source depth is 15 m and the frequency is 60 Hz.

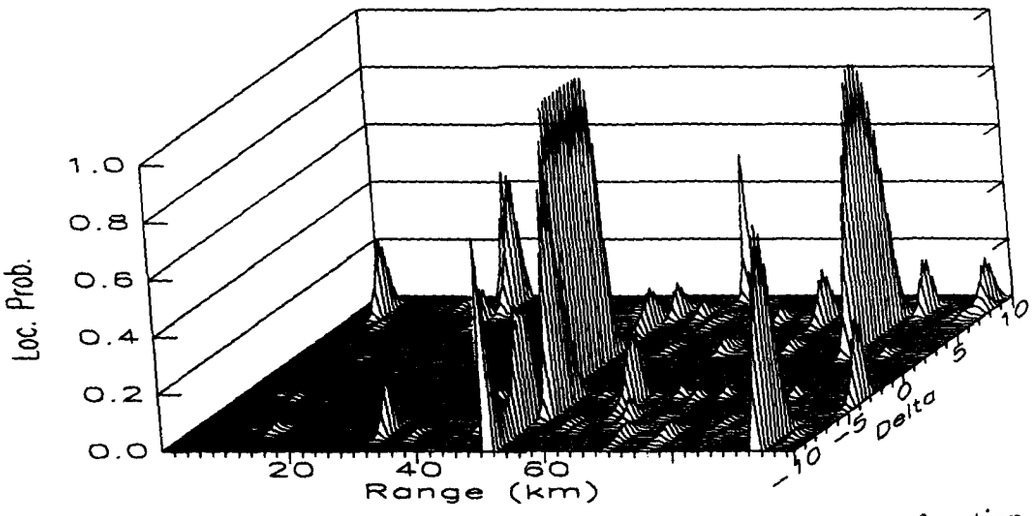

Figure 24: Mismatched-OMFP a posteriori range pdf output as a function of perturbation amplitude. The true source range is 50000 m. The source depth is 30 m and the frequency is 60 Hz.

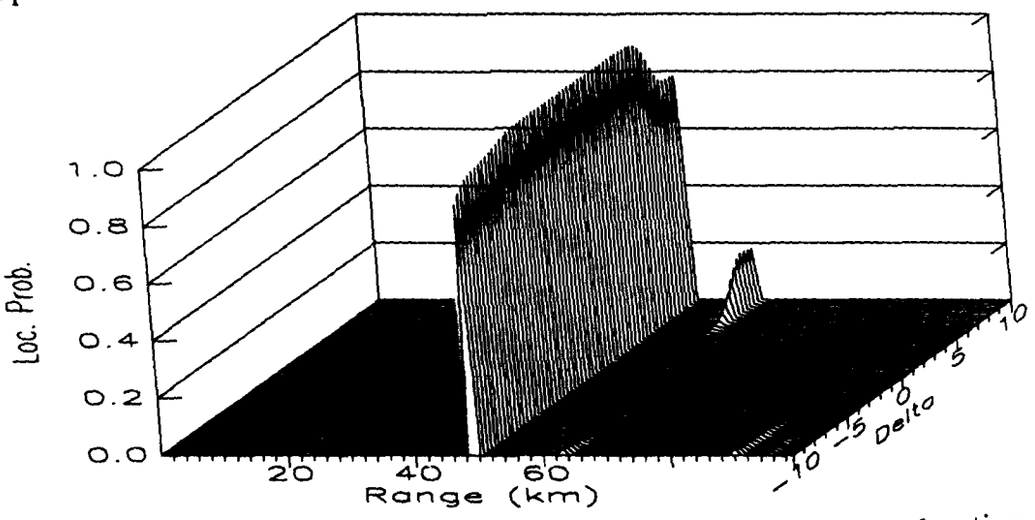

Figure 25: Mismatched-OMFP a posteriori range pdf output as a function of perturbation amplitude. The true source range is 50000 m. The source depth is 60 m and the frequency is 60 Hz.

the right location when the processor is matched, but the resolution is poor. As the value of c_p moves farther from zero (i.e., the mismatch between the designed environment and the actual environment becomes greater) the peak in the pdf shifts downward from the true source depth. Interestingly, the resolution increases.

Fig. 27 shows the corresponding output of the OUFP. The peak is in the right location for all values of the perturbation amplitude, but the resolution is poor.

Figs. 28 and 29 show the processor outputs after increasing the source frequency to 60 Hz. The mismatched-OMFP does a good job of determining the source depth for values of c_p near zero and for positive values of c_p, but the performance of the OUFP is clearly superior to that of the mismatched-OMFP for almost all values of c_p. The resolution of both processors is increased, due to the higher source frequency.

6.3 Summary

The performance of the mismatched-OMFP and the OUFP is dependent upon source position, the acoustic environment, and the frequency. The robust performance of the OUFP, relative to that of the mismatched-OMFP, was illustrated in several cases for realistic SVP pertrubations. At high frequencies the results indicate that mismatched-OMFP may be very sensitive to even small uncertainties in the SVP. The mismatched-OMFP is limited to applications in which the size of any uncertain SVP perturbations is a small fraction of the acoustic wavelength.

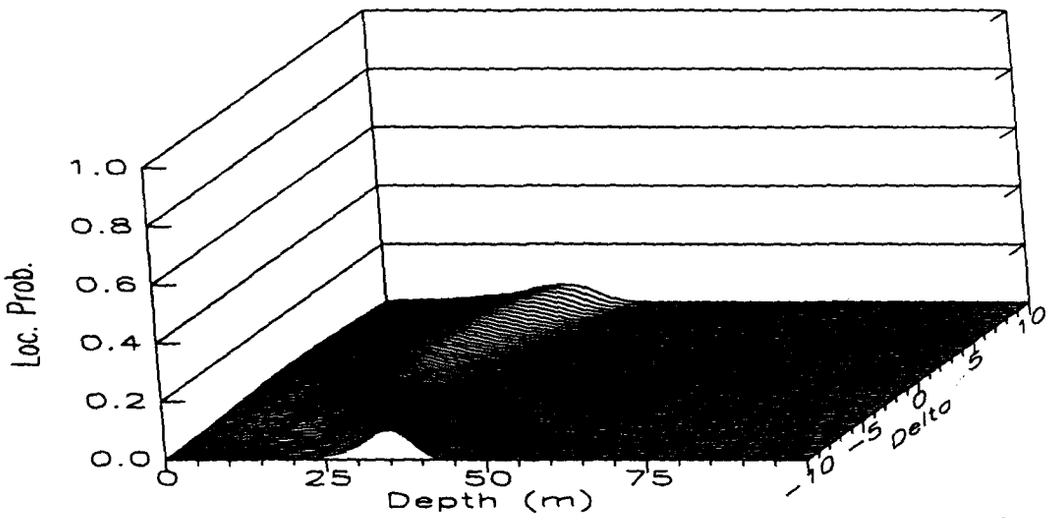

Figure 26: Mismatched-OMFP a posteriori depth pdf output as a function of perturbation amplitude. The true source depth is 15 m. The source range is 50000 m and the frequency is 15 Hz.

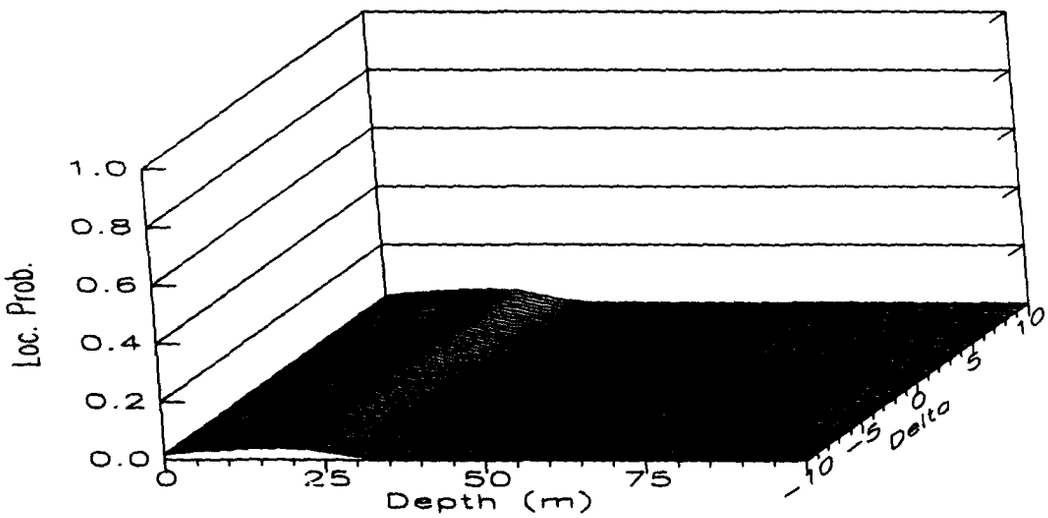

Figure 27: OUFP a posteriori depth pdf output as a function of perturbation amplitude. The true source depth is 15 m. The source range is 50000 m and the frequency is 15 Hz.

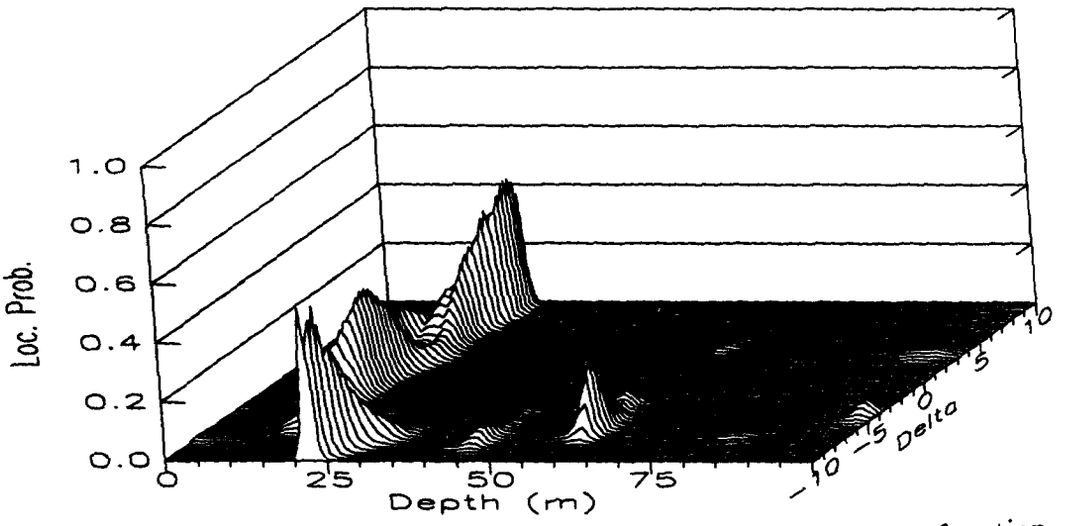

Figure 28: Mismatched-OMFP a posteriori depth pdf output as a function of perturbation amplitude. The true source depth is 15 m. The source range is 50000 m and the frequency is 60 Hz.

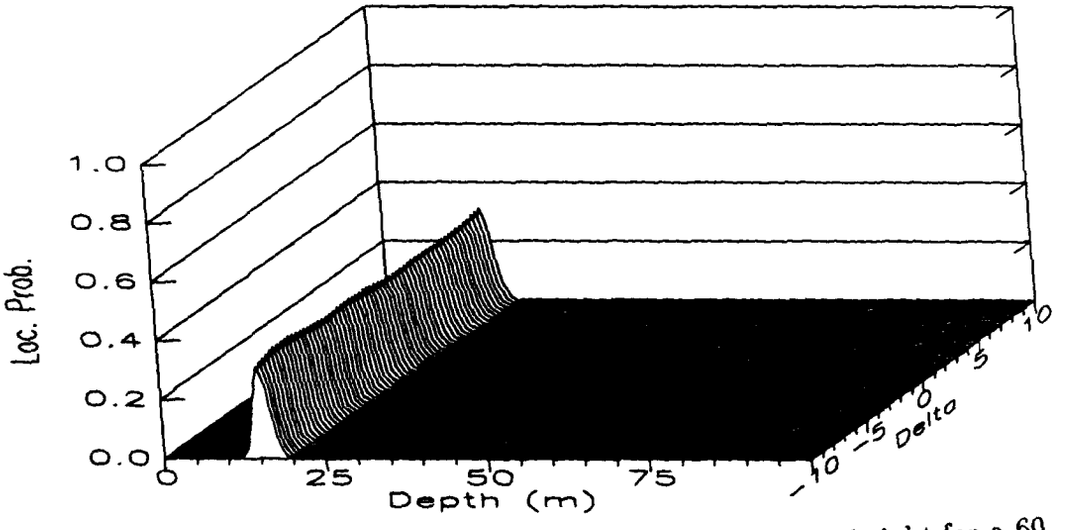

Figure 29: OUFP depth estimate sensitivity to perturbation height for a 60 Hertz source.

7 Results-Sensitivity to Range Dependent Perturbations

In this section we investigate and compare the sensitivity of matched field and uncertain field processing in a range-dependent acoustic environment [10, 11].

7.1 The Sound Velocity Profile Model

The range-dependent sound velocity profile is modeled as

$$c(z) = c_M(z) + c_p \exp\left(-\frac{1}{2}\left[(r - r_p)^2/\sigma_r^2 + (z - z_p)^2/\sigma_z^2\right]\right) \qquad (65)$$

where $c_M(z)$ is a Munk profile with parameters c_0 (axis sound speed) equal to 1500 m/s and z_0 (axis depth) equal to 1000 m. (This is the same profile used in the previous sections.) The second term represents a range-dependent Gaussian perturbation in the SVP with a peak at range r_p and depth z_p. The standard deviation width in range is σ_r while that in depth is σ_z. The sensitivity with respect to c_p is again investigated

The perturbation peak is placed at a range of 25000 meters from the source and at axis depth (1000 meters). The range standard deviation width is 5000 meters while the depth width is 250 meters. The height of the peak is varied between -5 and 5 meters/second.

7.2 Suboptimum Localization

The standard normal-mode model is not range-dependent, so the ray theory model is used to calculate the replica fields and the observation.

Calculation of the replica fields for the optimum uncertain field processor requires that a new ray trace be performed for each possible source position and each environment. The computer processing time is prohibitive for any problems of interest.

Instead of examining the performance of the range-dependent optimum uncertain field processor we look at three suboptimum range-independent processors. These suboptimum processors use range-independent ray tracing to calculate the replica fields. (The principle of *acoustic reciprocity* can be applied in a range independent environment to greatly reduce the number of ray traces that have to be done to compute the replica fields. Replica

fields corresponding to the same source depth and environment, but different ranges, can be computed from the same ray trace.) Since the actual environment is range-dependent, none of the suboptimum processors can calculate a replica field which exactly matches the observed field.

The first suboptimum processor is the mismatched optimum matched field processor (mismatched-OMFP). This processor is matched to the range independent environment which exists in the absence of the perturbation.

The second suboptimum processor is the mismatched optimum uncertain field processor (mismatched-OUFP). It calculates replica fields from range-independent profiles which have a Gaussian perturbation at the axis depth. The height of this perturbation is assumed unknown and uniformly distributed between -2 and 2 meters/second. Since the actual range averaged profile lies within this region of uncertainty it is hoped that good performance can be achieved with this processor. (If the actual perturbation height is 5 meters/second, the range averaged profile (average out to 75000 meters) is a Munk profile with Gaussian perturbation of height 0.8 meters/second.) Note that this processor is an uncertain field processor, but it doesn't use *the correct uncertain environment.*

The third suboptimum processor is a new uncertain field processor. It averages conventional ambiguity functions which result from different replica fields. The average is calculated over the same range-independent profile uncertainty as used by the mismatched-OUFP. This processor is termed mismatched supoptimum uncertain field processor (mismatched-SUFP).

7.3 Estimation Sensitivity

The same 10 element array used in previous sections is used here. The source is on axis (1000 m) and at a range of 75000 m. The frequency is 100 Hertz. The detection factor is 93 dB.

7.3.1 Range Estimation

We consider the problem of estimating only the range coordinate when the source depth is known.

The mismatched-OMFP output as a function of actual perturbation height is shown in Fig. 30. Note that when c_p (labelled Delta in the figure) is zero the actual environment is range-independent and the mismatched-OMFP is

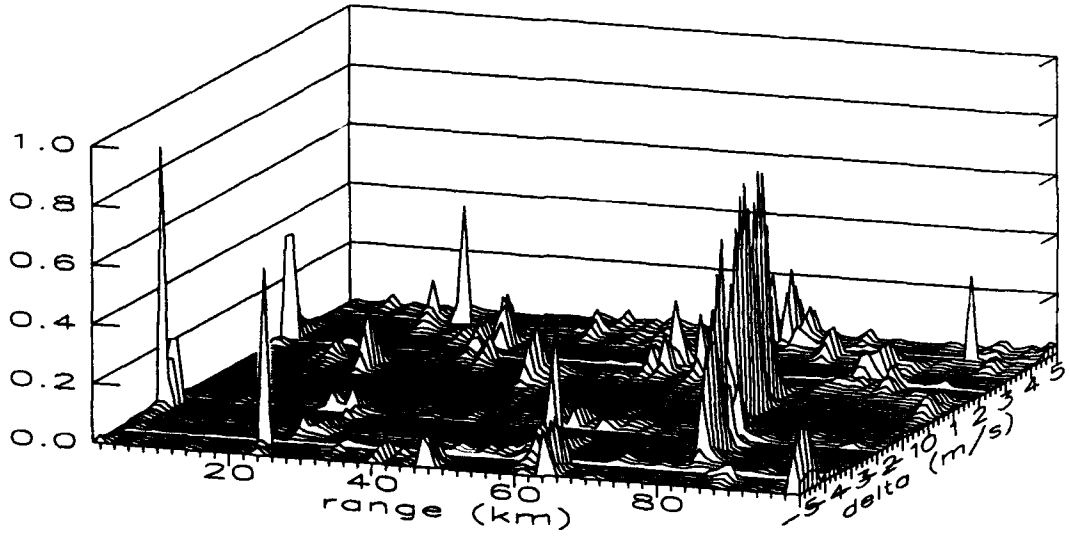

Figure 30: Mismatched-OMFP a posteriori range pdf output as a function of perturbation amplitude. The true source range is 75000 m.

matched to the environment. In this region strong peaks near the true source range of 75000 m can be observed. When the absolute value of the actual perturbation height is greater than about 2 m/s ambiguities appear in the output and localization performance decreases rapidly.

The output of the mismatched-OUFP is shown in Fig. 31. This processor performs slightly better than the previous one. Some of the large spurious peaks have been suppressed and the ridge at 75000 m is slightly wider.

The output of the mismatched-SUFP is shown in Fig. 32. The performance of this processor is quite poor for almost all values of the perturbation amplitude. The figure illustrates that seemingly reasonable ad hoc approaches to the design of localization algorithms may result in processors with very poor performance.

7.3.2 Depth Estimation

We now consider the problem of estimating the depth coordinate when the range is known.

The output of the mismatched-OMFP as function of perturbation height is shown in Fig. 33. There is a peak at the true source depth when the

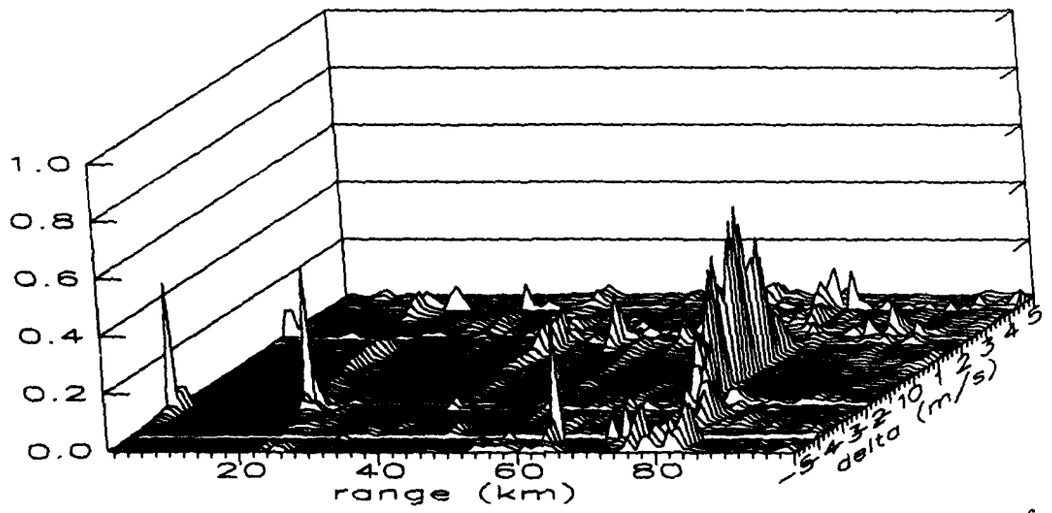

Figure 31: Mismatched-OUFP a posteriori range pdf output as a function of perturbation amplitude. The true source range is 75000 m.

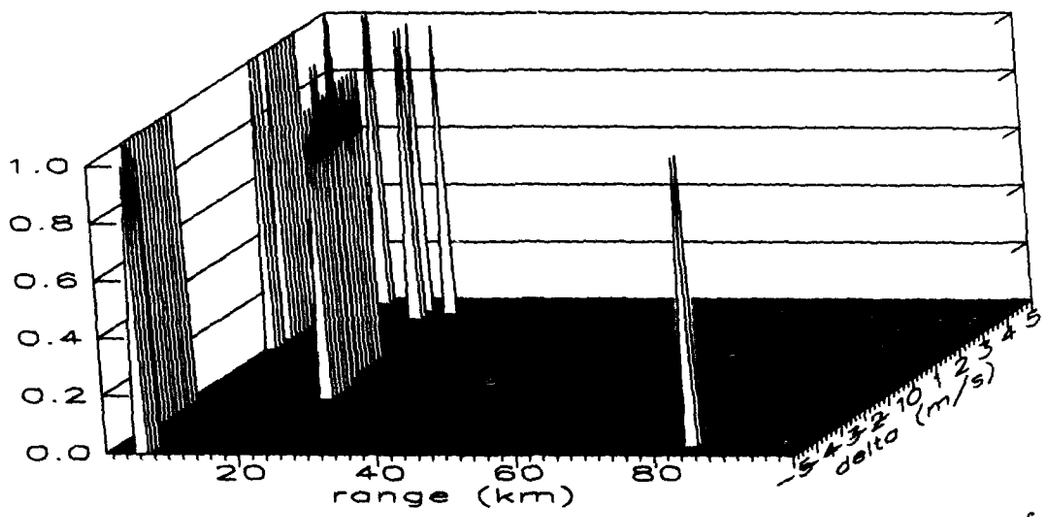

Figure 32: Mismatched-SUFP a posteriori range pdf output as a function of perturbation amplitude. The true source range is 75000 m.

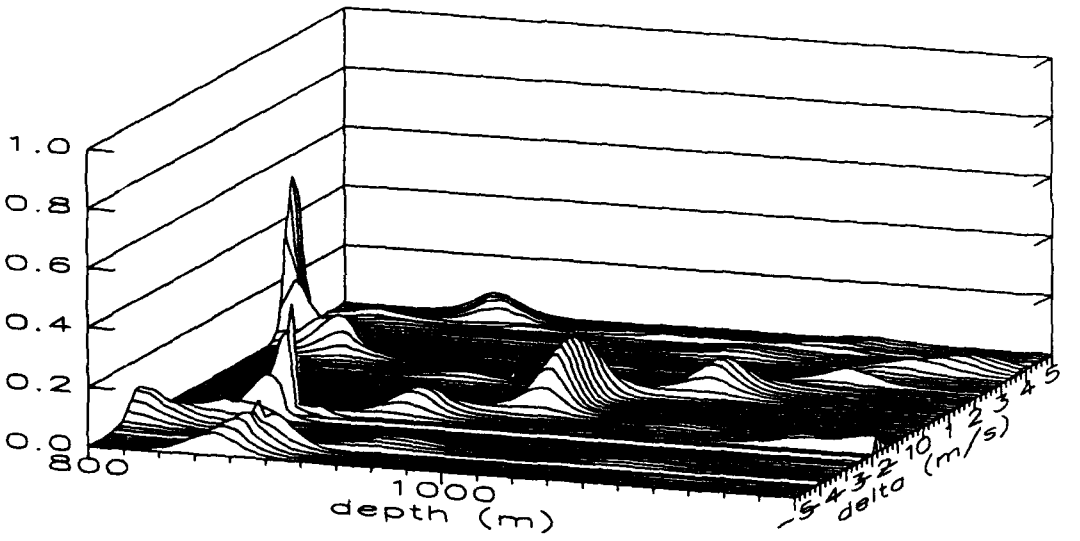

Figure 33: Mismatched-OMFP a posteriori depth pdf output as a function of perturbation amplitude. The true source depth is 1000 m.

perturbation amplitude is zero (no mismatch), but the peak of the pdf shifts away from the true depth as the perturbation amplitude moves away from zero. The peak in the pdf appears at a depth almost 200 m away from the true depth ath the extreme values of the perturbation amplitude.

The corresponding output of the mismatched-OUFP is shown in Fig. 34. The performance improvement over the mismatched-OMFP case is more noticeable here than in the range estimation case. Some spurious peaks are present in the figure, but there is a ridge very near the true source depth across all values of the perturbation amplitude.

The mismatched-SUFP output is shown in Fig. 35. This processor performs much better, relative to the mismatched-OMFP, than in the range estimation case. A ridge appears at the correct depth over the portion of the figure near where the perturbation amplitude is zero, but large spurious peaks appear away from the true source depth as the perturbation amplitude increases.

To put the performance of these suboptimum processors in perspective, the output of the optimum uncertain field processor for this environment is shown in Fig. 36. This processor assumes the environment is range-dependent

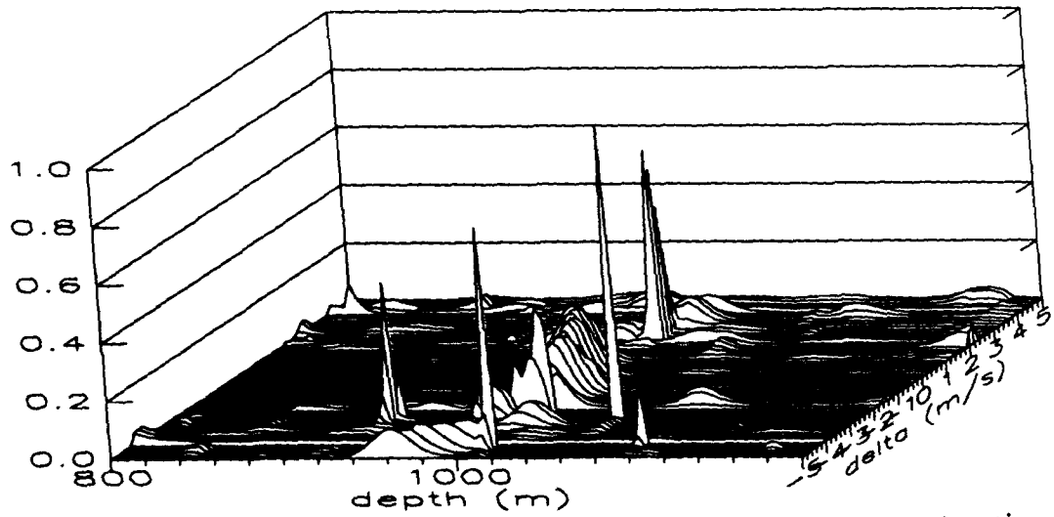

Figure 34: Mismatched-OUFP a posteriori depth pdf output as a function of perturbation amplitude. The true source depth is 1000 m.

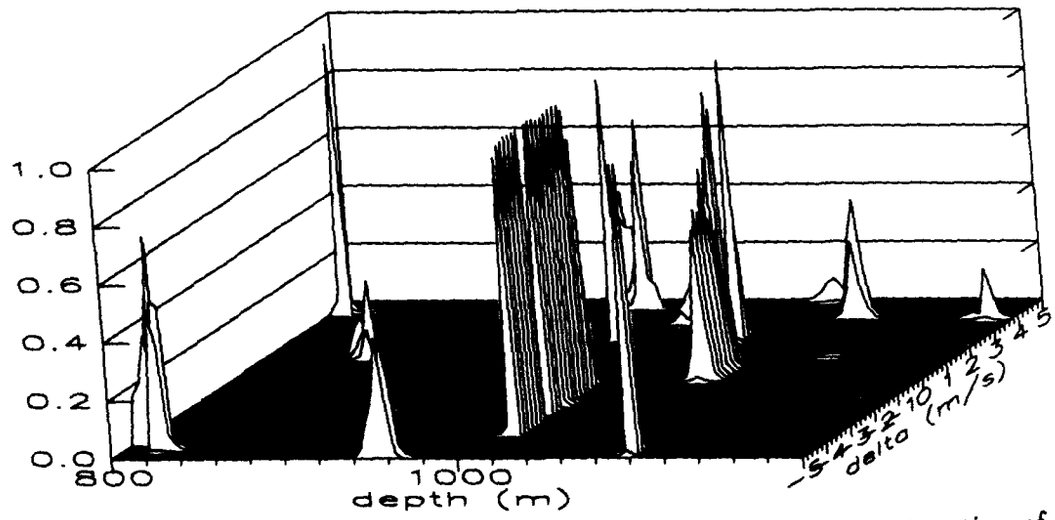

Figure 35: Mismatched-SUFP a posteriori depth pdf output as a function of perturbation amplitude. The true source depth is 1000 m.

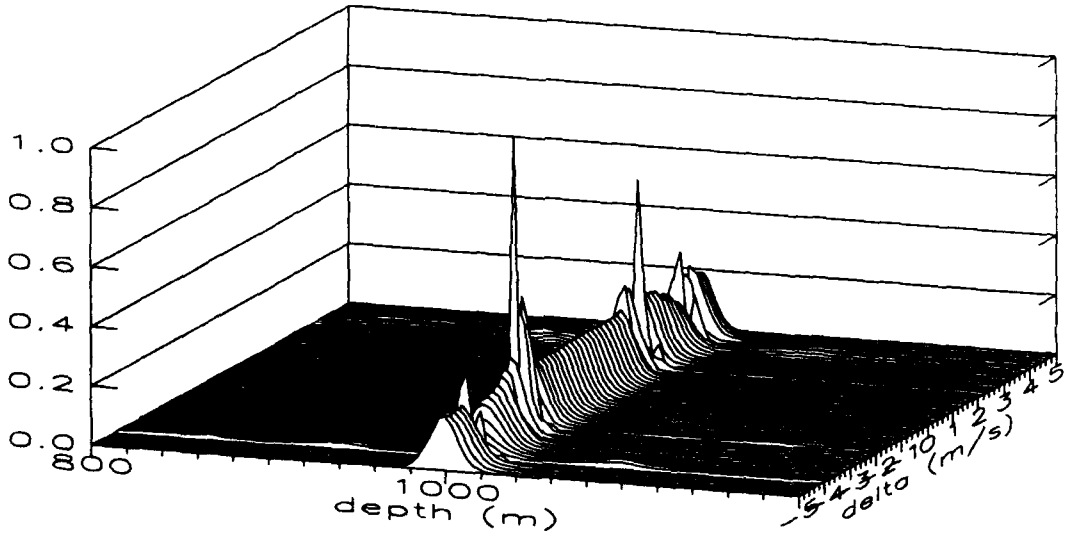

Figure 36: OUFP a posteriori depth pdf output as a function of perturbation amplitude. The true source depth is 1000 m.

with a Gaussian perturbation of unknown amplitude. The range-dependent acoustic ray propagation model is used to calculate the replica fields. The optimum processor is quite robust with respect to uncertainty in the perturbation height.

7.4 Summary

In this section we've compared the performance of three suboptimum processors. The three processors used a range-independent propagation model to calculate the replica fields, although the actual environment is range-dependent. The suboptimum processor which is based on the optimum uncertain field processor had the best performance. Although this processor doesn't perform as well as the optimum, the reduced processing time requirements make it an attractive alternative to the optimum in some situations.

References

[1] H. P. Bucker, Use of calculated sound fields and matched-field detection to locate sound sources in shallow water. *J. Acoust. Soc. Am.*, 59:368, 1976.

[2] R. S. Clarke, Range-depth and range-angle localization of an ocean acoustic source, M. S. thesis, Duke University, December 1989.

[3] Donald R. DelBalzo, CHristopher Feuillade, and Mary M. Rowe. Effects of water-depth mismatch on matched-field localization in shallow water. *J. Acoust. Soc. Am.*, page 2180, 1988.

[4] J. V. DiFranco and W. L. Rubin, *Radar Detection*, Artech House, Inc., 610 Washington Street, Dedha;m, Mass. 02026, 1980.

[5] C. Nelson Dorny, *A Vector Space Approach to Models and Optimization*, Robert E. Krieger Publishing Company, Huntington, New York, 1980.

[6] M. B. Porter, R. L. Dicus, and R. G. Fizell, Simulations of matched-field processing in a deep-water pacific environment, *IEEE J. of Oceanic Eng.*, OE-12:173, 1987.

[7] I. S. Gradshteyn and I. M.Ryzhik, *Table of Integrals, Series, and Products*, Academic Press, Orlando, 1980.

[8] H. A. Lazoff, Underwater detection performance and sensitivity to sound velocity profile variations, M. S. thesis, Duke University, March 1989.

[9] Michael Porter and Edward L. R iss, A numerical method for ocean-acoustic normal modes. *J. Acoust. Soc. Am.*, 76:244-252, July 1984.

[10] A. M. Richardson and L. W. Nolte, A posteriori probability source localization in an uncertain sound speed, deep ocean environment, *J. Acoust. Soc. Am.*, 89:2280-2284, May, 1991.

[11] A. M. Richardson, Optimal localization of ocean acoustic sources in an uncertain environment, Ph. D. thesis, Duke University, September, 1990.

[12] N. A. Rausch, Underwater signal estimation: performance comparison of two processor methods, M. S. thesis, Duke University, December 1989.

[13] A. Tolstoy, Sensitivity of matched field p;rocessing to sound-speed profile mismatch for vertical arrays in a deep water pacific environment, *J. Acoust. Soc. Am.*, 85:2394, 1989.

[14] Robert J. Urick, *Principles of Underwater Sound*, McGraw-Hill, Inc., New York, third edition, 1983.

8 Participating Scientific Personnel

- Howard A. Lazoff, "Ocean Acoustic Detection Performance and Sensitivity to Sound Speed Profile Variations," Ph.D. student, Duke University.
- Nancy Rausch, "Ocean Acoustic Source Localization," M.S. Thesis, Duke University, December, 1989.
- Robert Clarke III, "Range-Depth and Range Angle Localization of an Ocean Acoustic Source," M.S. Thesis, Duke University, December, 1989.
- Anthony M. Richardson, "Optimal Localization of Ocean Acoustic Sources in an Uncertain Environment," Ph.D. Thesis, Duke University, September, 1990.

9 Publications and Papers

- A. M. Richardson and L. W. Nolte, "Performance and Sensitivity of Matched Field and Uncertain Field Processor Approaches", *Meeting of the Acoustical Society*, State College, Pennsylvania, May 1990.
- A. M. Richardson and L. W. Nolte, "Source Localization in an Uncertain Range- Dependent Ocean", OCEANS 90 Conference, Arlington, Virginia, September, 1990.
- A. Reibman and L. W. Nolte, "Optimal Fault-tolerant Signal Detection," *IEEE Transactions on Acoustics, Speech, and Signal Processing*, Vol. 38, Issue 1, pp. 179-181, January 1990.
- A. R. Reibman and L. W. Nolte, "Optimal Design and Performance of Distributed Signal Detection Systems with Faults," *IEEE Transactions on Acoustics, Speech and Signal Processing*, Vol. 38, Issue 10, pp. 1771-1782, October, 1990.